Reaction Chemical Kinetics in Biology

Chapter · March 2019

DOI: 10.1002/9781119483977.ch9

2 authors:

Nicholas J Harmer
University of Exeter
113 PUBLICATIONS **2,443** CITATIONS
SEE PROFILE

Mirella Vivoli Vega
University of Bristol
47 PUBLICATIONS **705** CITATIONS
SEE PROFILE

9

Reaction Chemical Kinetics in Biology

Nicholas J. Harmer[1] *and Mirella Vivoli Vega*[2]

[1] *Living Systems Institute, University of Exeter, Stocker Road, Exeter, EX4 4QD, UK*
[2] *Department of Biomedical Experimental and Clinical Sciences, University of Florence, Viale Morgagni 50, 50134 Florence, Italy*

9.1 Significance

The function of many proteins is to act as catalysts for biological reactions. These protein catalysts, *enzymes*, generally speed up the rate of one or at most a few reactions, with a limited range of potential substrates. There is a general scientific interest in quantitatively understanding how enzymes alter the rate of reactions. Quantifying how reaction rates change underpins our understanding of cellular physiology; for industrial usage, it is critical to know how fast reactions will take place and there is an increasing interest in using synthetic biology to engineer new biochemistry into organisms. Enzyme assays have been foundational to our understanding of biology in the past and will contribute to an even broader range of applications in the next wave of biological sciences.

9.1.1 Examples of Enzyme Use (Clinical and Biotechnology)

Defects in enzymes underlie many human genetic conditions. Two of the most common human homozygous genetic defects in enzymes are mutations in the enzymes phenylalanine 4-hydroxylase (PAH; Figure 9.1a) [4, 5] and glucose-6-phosphate dehydrogenase (G6PD; Figure 9.1b) [6]. PAH hydroxylates phenylalanine to tyrosine as part of the phenylalanine catabolism pathway (KEGG pathway map 00360 [7]). Reduction in the rate of this enzyme leads to an accumulation of phenylalanine in the blood (hyperphenylalaninemia). This leads to the clinical symptoms of phenylketonuria (PKU). Prevention of PKU is now achieved by testing newborns for elevated phenylalanine via a heel prick test [4, 5]. Understanding of the PAH enzyme's structure and enzymology have allowed PAH function to be substantially restored in approximately 20% of patients by use of the modified *cofactor*[1] sapropterin dihydrochloride [8] that promotes enzyme folding and function. G6PD oxidises glucose-6-phosphate as one of the two NADPH generating steps in the pentose phosphate pathway (Figure 9.1b). Over 200 disease causing mutations are currently known [9]. G6PD deficiency is generally treated by management: the genetic defects are generally sufficiently minor to be asymptomatic in the absence of haemolytic or oxidative stressors [6]. Testing for G6PD levels is routine before a selection of drugs are prescribed, as these drugs act as such stressors [10, 11]. Firm diagnosis of G6DH deficiency is achieved through an enzyme assay for activity levels in red blood cells [12]. An accurate quantitative assay is essential as disease penetrance and symptoms correspond closely to residual enzyme activity.

1 *Cofactors* are metal ions or small molecules (e.g. haem, NAD^+) that form part of the enzyme and are required for the function of the enzyme. Some are catalytic (e.g. metal ions), while others must be regenerated by other cellular systems (e.g. glutathione).

Biomolecular and Bioanalytical Techniques: Theory, Methodology and Applications, First Edition. Edited by Vasudevan Ramesh.

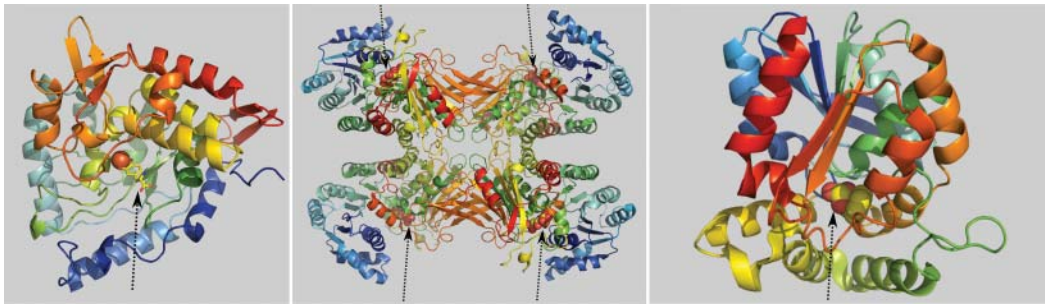

Figure 9.1 Examples of enzymes important to health and industry. Enzymes are shown as cartoon (rainbow colours: N-terminus blue, C-terminus red); ligands are shown as spheres or sticks (carbon: yellow; oxygen: red; nitrogen: blue; iron: brown). (a) Phenylalanine 4-hydroxylase catalytic domain, with the (catalytic) iron and inhibitor L-DOPA (3,4-dihydroxyphenylalanine; sticks, dashed arrow) highlighted. (b) Glucose 6-phosphate dehydrogenase tetramer, with glucose 6-phosphate (dashed arrows). (c) γ-lactamase monomer, with a substrate analogue (dashed arrow). Images generated using PyMOL from RCSB PDB IDs: 6PAH [1], 5UKW [2], 1HL7 [3].

Another key use of enzymes is in the manufacturing of high value chemicals, such as drug molecules and perfumes [13, 14]. Enzymes offer many advantages for chemical synthesis, including high specificity, high reaction yields, strong stereo- and regio-selectivity, and the potential to combine several reaction steps [15, 16]. Enzymes can be readily incorporated into very small reactors for syntheses on a micro or nanoscale [17], facilitating efficient synthesis at all scales. For example, γ-lactamases (Figure 9.1c) allow the enantiomeric resolution of the bicyclic lactam 2-azabicyclo[2.2.1]hept-5-en-one, a key building block for antivirals (e.g. carbovir) [18]. The major drawback that has restricted the use of enzymes on a wider scale has been their high specificity. Together with the limited tolerance to heating and solvents that most enzymes display, this makes finding suitable enzymes for industrial biotransformations difficult. These challenges are being overcome by a combination of directed evolution, protein design and semi-rational mutagenesis. The capacity to rapidly test many protein variants is the major bottleneck of these methods. Obtaining the right industrial properties requires elegantly designed enzyme assays to provide sensitivity and throughput at the very high levels required.

9.2 Overview of Kinetics and Its Application to Biology

Enzyme kinetics represents one branch of the broader field of chemical kinetics [19]. This field includes investigations of the relationship between the concentration of a substrate in a reaction and the rate of the reaction. For a chemical reaction, the *rate* (the change in concentration of the reactants or products) is generally related to the concentration of the reactants by a simple power law. Depending on the nature of the reaction, this may be zero order (substrate concentration does not affect the reaction), first order (rate is proportional to substrate concentration) or second order (rate is proportional to the square of substrate concentration; Figure 9.2). Higher order reactions are rarer, but do occur [19]. For reactions with multiple substrates, the reaction rate will be zero, first or second order with respect to each substrate: again, the overall order of the reaction is usually second order or less.

Enzyme kinetics have a greater level of complications. These arise because the enzyme catalyst is a highly complex molecule and undergoes structural changes on a very rapid (nanosecond to microsecond) timescale. The enzyme reaction usually occurs on a microsecond to second timescale and includes many steps (including substrate binding, the formation of intermediates and the release of products). Consequently, the process by which the enzyme speeds up the reaction must be considered to understand the nature of the catalytic process and the relevant kinetic parameters.

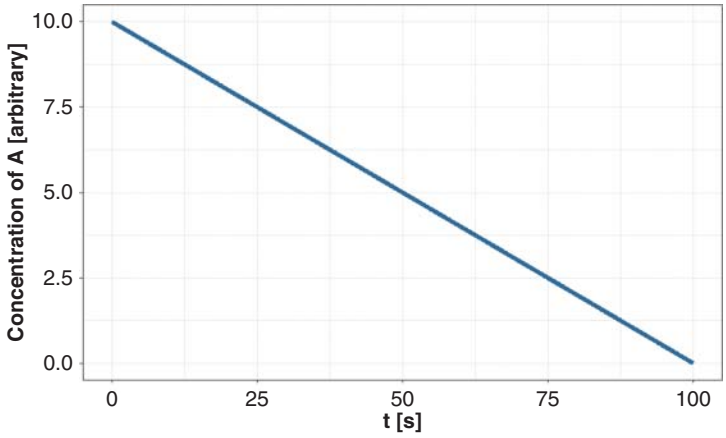

(a)

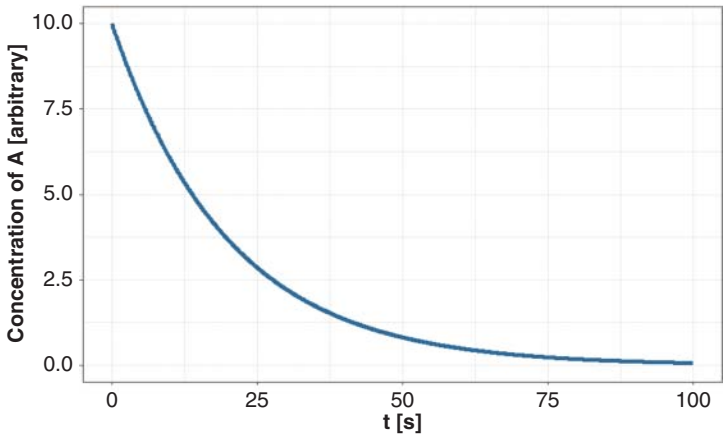

(b)

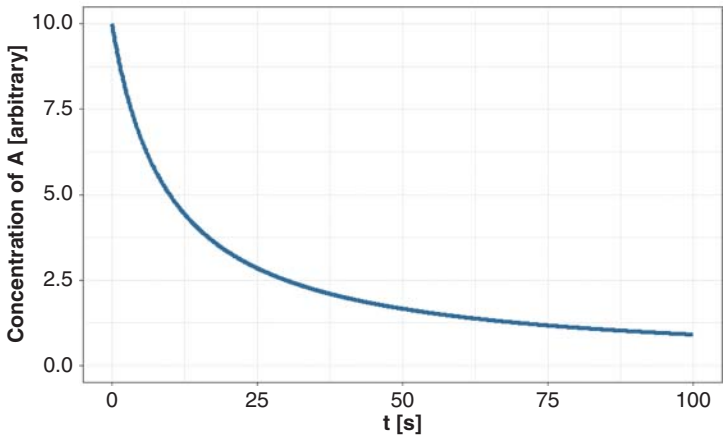

(c)

Figure 9.2 Reactions with different orders with respect to the substrate. In each case, the concentration of substrate *A* is shown reducing from an arbitrary starting point, over an arbitrary time period. (a) Zero-order reaction. Here, the reduction in concentration of *A* shows no dependence on the substrate concentration. (b) First-order reaction. In this case, the rate of the reaction (and so consumption of *A*) is directly proportional to the concentration of *A*. The rate slows considerably as *A* is consumed. (c) Second-order reaction. The rate of reaction is related to the square of the concentration of *A* (e.g. two molecules of *A* combining to form some product). The reaction initially proceeds rapidly, but falls significantly as the concentration of *A* approaches zero.

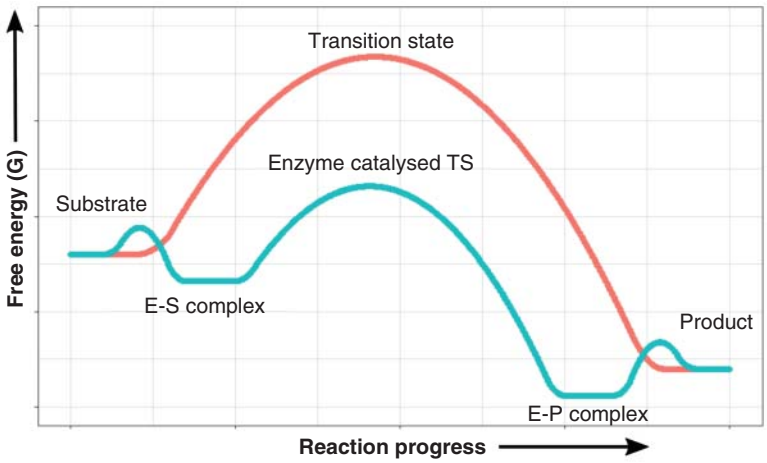

Figure 9.3 Schematic of enzyme catalysis. The uncatalysed reaction (red) has to overcome a large free energy barrier to reach the transition state (TS). A simple example enzyme catalysed reaction (blue) provides a reaction route at a lower free energy. The free energy barrier is lower, allowing more molecules to react. The reaction is more complicated, with enzyme-substrate (E-S) and enzyme-product (E-P) complexes.

The nature of enzyme catalysis is to provide a reaction pathway with a lower free energy barrier than the uncatalysed reaction (Figure 9.3). Most enzyme-catalysed reactions take place at a very slow rate in the absence of catalysis. All reactions must pass through one or more *transition state(s)* that are maxima in free energy. The rate of the reaction will be determined by the proportion of substrate molecules that are able to access this state. In order to access the enzyme-catalysed intermediate state, the substrate must first bind to the enzyme. As binding of substrate to the enzyme is usually a fast, reversible event, the rate of these reactions is far too rapid to be determined except with specialist instruments designed to collect rate data on millisecond timescales (see *Advanced Methods*, Section 9.6).

9.2.1 Steady-State Kinetics

Most enzymology studies instead use *steady-state kinetics*. These are measured on a seconds to minutes timescale and so can be studied using widely available instruments. The assumption of a steady state (see below) allows the simplification of the reaction scheme. The resulting kinetic equation is familiar to most biological sciences and bioorganic chemistry students from an early part of their studies.

The *Michaelis–Menten equation* (Eq. (9.1)) is derived using a model of an enzyme with a single substrate and a single product. There is a single step between each of the following states: free enzyme and substrate; enzyme–substrate complex; enzyme–product complex; and free enzyme and product. The transitions between each of these states is determined by a rate constant in either direction (Figure 9.4). To determine all of these rate constants would require a large quantity of data, including data at millisecond timescales, as the binding and release of both substrate and product from the enzyme is likely to take place on such timescales.

$$v = \frac{V_{max}\,[S]}{K_M\,[S]}, \tag{9.1}$$

where V is the initial reaction rate, V_{max} is the reaction rate at infinite substrate concentration, $[S]$ is the substrate concentration and K_M is the Michaelis constant.

Deriving the Michaelis–Menten equation relies on assumptions to simplify the scheme. The reaction is assumed to be unidirectional (i.e. $k_{-2} = 0$) and the product release is assumed to be fast and irreversible ($k_3 = \infty$, $k_{-3} = 0$). These assumptions are most reasonable when the product concentration is zero or low, and simplify the reaction scheme considerably (Figure 9.4b).

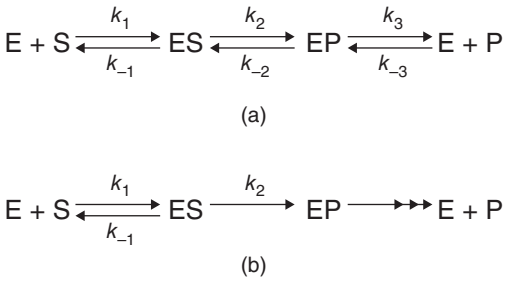

Figure 9.4 Reaction scheme for an enzyme (E) catalysed reaction with one substrate (S) and one product (P). (a) Each reaction is modelled as reversible in the general case. Each step has a rate constant (k_1, k_{-1}, etc.). (b) Simplified scheme. The conversion from the enzyme–substrate complex to an enzyme-product complex is considered irreversible and the release of product is considered to take place considerably faster than this conversion. This considerably reduces the complexity of the system, simplifying experimental determination.

Secondly, the *steady state approximation*, introduced by Briggs and Haldane [20], is applied. It is assumed that as the reaction progresses, it will rapidly reach a state where the rate of formation and breakdown of the enzyme–substrate complex (the remaining intermediate in the reaction) will become equal. The consequence of this is that there is no change in the concentration of the enzyme–substrate complex (Eq. (9.2)). Modelling a generic reaction demonstrates that this rapidly becomes true and that this is true for reactions across a wide range of reasonable values for k_1 and k_{-1} (Figure 9.5). The steady-state approximation is given as

$$k_1\,[E][S] = k_{-1}\,[ES] + k_2\,[ES]. \tag{9.2}$$

In most experiments, the substrate concentration will considerably exceed the enzyme concentration and so the formation of the enzyme–substrate complex will have no real effect on the substrate concentration. However, there will be a significant effect on the enzyme concentration. The enzyme concentration will no longer be the initial concentration added to the experiment:

$$[E] = [E_0] - [ES]. \tag{9.3}$$

Combining (9.2) and (9.3):

$$k_1\,[S]\,([E_0] - [ES]) = k_{-1}\,[ES] + k_2\,[ES]. \tag{9.4}$$

Rearranging (9.4):

$$k_1\,[S]\,[E_0] = k_{-1}\,[ES] + k_2\,[ES] + k_1[S][ES], \tag{9.5}$$

$$k_1\,[S]\,[E_0] = (k_{-1} + k_2 + k_1[S])\,[ES], \tag{9.6}$$

$$\frac{k_1\,[S]\,[E_0]}{k_{-1} + k_2 + k_1[S]} = [ES], \tag{9.7}$$

$$\frac{[S]\,[E_0]}{\frac{k_{-1}+k_2}{k_1} + [S]} = [ES]. \tag{9.8}$$

Equations (9.3) to (9.8) are rearrangements of the steady-state approximation to define $[ES]$.

In a simplified scheme for the reaction (Figure 9.3b), the observed rate of the reaction will be equal to the rate at which product P is generated:

$$\frac{\mathrm{d}[P]}{\mathrm{d}t} = k_2\,[ES] = v. \tag{9.9}$$

Equation (9.9) is a statement of the rate of the reaction.

Substituting the enzyme–substrate complex determination from (9.8) into (9.9) gives

$$v = \frac{k_2\,[E_0][S]}{\frac{k_{-1}+k_2}{k_1} + [S]}. \tag{9.10}$$

Equation (9.10) is the derived Michaelis–Menten equation following Briggs and Haldane [20].

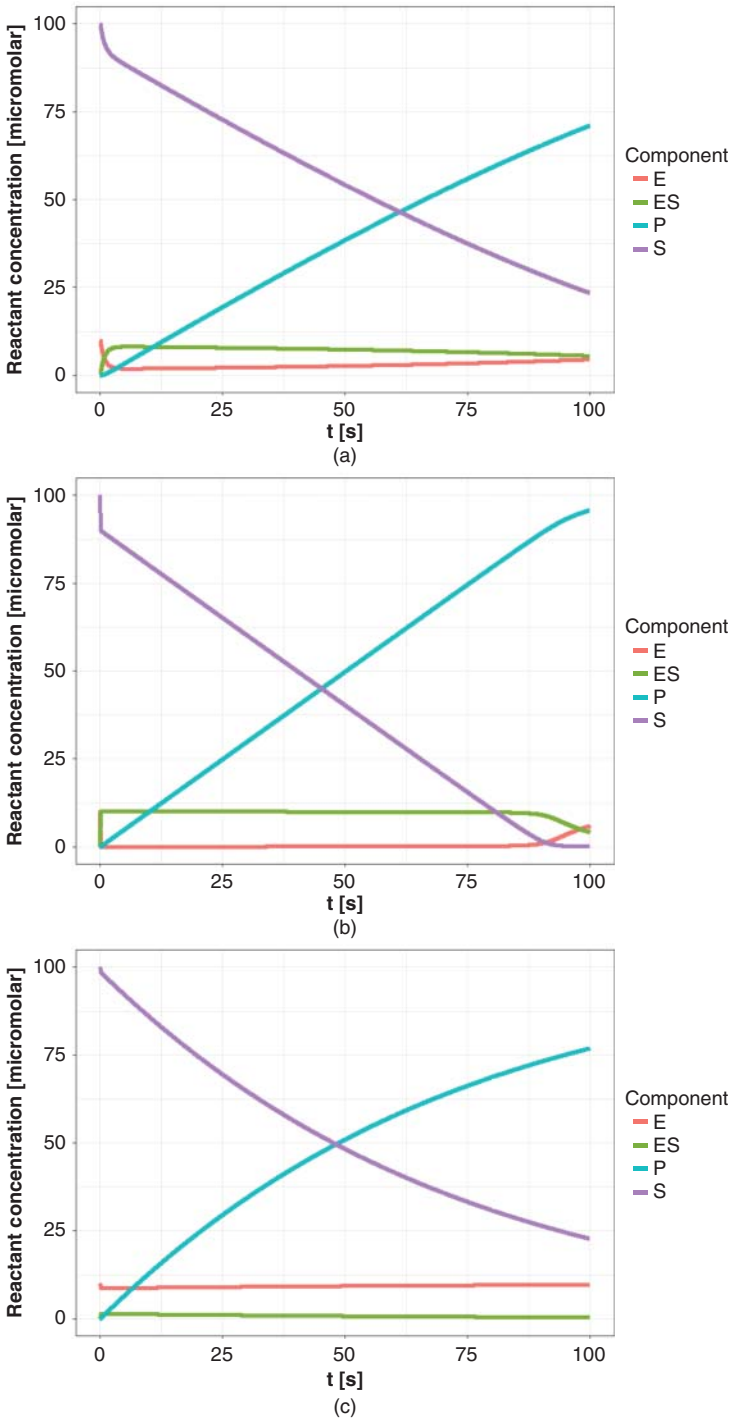

Figure 9.5 The steady state approximation. Simulations are shown for a simple unisubstrate enzyme obeying the approximation in Figure 9.3b. A high enzyme concentration is used so that the ES complex concentration is on the same scale as the substrate and product. Three scenarios are illustrated to demonstrate that the steady-state approximation holds across a range of K_M. (a) Approximating average K_M, the steady state holds with a slow drop in concentration after the initial phase of the reaction. (b) Approximating low K_M (high k_1), the steady state is maintained until the reaction is almost complete. (c) Approximating high K_M (low k_1; higher k_{-1}), the ES complex concentration reduces once the initial phase (10–20% of substrate exhausted) is complete.

We now define $V_{max} = k_2\,[E_0]$ and $K_M = (k_{-1} + k_2)/k_1$. Substituting these into Eq. (9.10) recovers Eq. (9.1), the form in which this is most commonly presented.

By considering how the Michaelis–Menten equation is derived, important points regarding an enzyme that follows these equations can be observed. Firstly, the rates obtained are only valid during the early parts of the reaction, as the assumptions made include the fact that there is no product. This is particularly the case for reversible reactions, as the reverse reaction will start to take place at a significant rate as product levels increase. Consequently, while this is not always practical, it is ideal to determine the rate of the reaction during the first 10% of substrate usage. Secondly, the steady-state approximation implies that firstly there will be a lag phase before the reaction reaches its maximum rate and that the rate of the reaction will then remain similar (in the absence of product effects) over a significant timeframe (Figure 9.5). Therefore, for many reactions, a certain 'dead-time' between the experimental setup and measurement can be tolerated. Careful choice of the amount of enzyme used will allow the reaction to proceed sufficiently slowly to allow the time required for measurements to be started and collection of data points to be made.

There are several other treatments that use similar assumptions but a different mathematical scheme. These also arrive at the same general equation. These alternative treatments are often used in more complicated situations (e.g. with multiple substrates) as they make the determination of rate equations more convenient. These treatments are reviewed in detail in more specialist texts [19, 21, 22].

9.2.2 Beyond the Michaelis–Menten Equation

9.2.2.1 Enzyme Cooperativity

There are several common scenarios where modification of the Michaelis–Menten equation is necessary. An important example is *cooperative enzymes* [23]. Cooperative enzymes show responses to ligands that are either sigmoidal (positive cooperativity; Figure 9.6a) or are hyperbolic (like Michaelis–Menten enzymes), with a more pronounced plateau at high ligand concentrations (negative cooperativity; Figure 9.6b). Both positive and negative cooperativity are common [24]. It is also likely that more enzymes are cooperative than is generally appreciated, with many being considered as Michaelis–Menten due to a scarcity or lack of sensitivity in the data (e.g. [25]).

Cooperativity was traditionally understood in the context of multimeric enzymes. In such enzymes, binding of substrate to one active site makes the binding of substrate to another active site more likely (positive cooperativity) or less likely (negative cooperativity; Figure 9.6). There are also cases of enzymes that display both positive and negative cooperativity [25–28]. Cooperative kinetics – especially positive cooperativity – is also observed in many monomeric enzymes [29]. Such enzymes generally adopt a low activity state in the absence of substrate, which switches slowly into a high activity state (where substrate binding occurs). Cooperative kinetics should therefore be considered for monomeric as well as multimeric enzymes.

Steady-state kinetics can also be studied for cooperative enzymes. There are several models available for understanding cooperative kinetics [30]. Classically, the two dominant hypotheses were the cooperative (Monod–Wyman–Changeux) and sequential (Koshland–Némethy–Filmer) models [31, 32]. Many enzymes display features of both models, and these likely represent two extremes of a spectrum of enzyme behaviour [19, 33]. As both models require several additional fast kinetic steps or equilibria, cooperative enzymes are usually fitted instead to a variation of the *Hill equation*, applied to Michaelis–Menten kinetics [19] (Eq. (9.11)). Positively cooperative enzymes will show $h > 1$, while negatively cooperative enzymes will show $h < 1$:

$$v = \frac{V_{max}\,[S]^h}{(K_{1/2}^h + [S]^h)}, \tag{9.11}$$

where $K_{1/2}$ is the substrate concentration at half-maximal enzyme rate and h is the Hill coefficient. When $h = 1$, the equation reverts to the standard Michaelis–Menten equation.

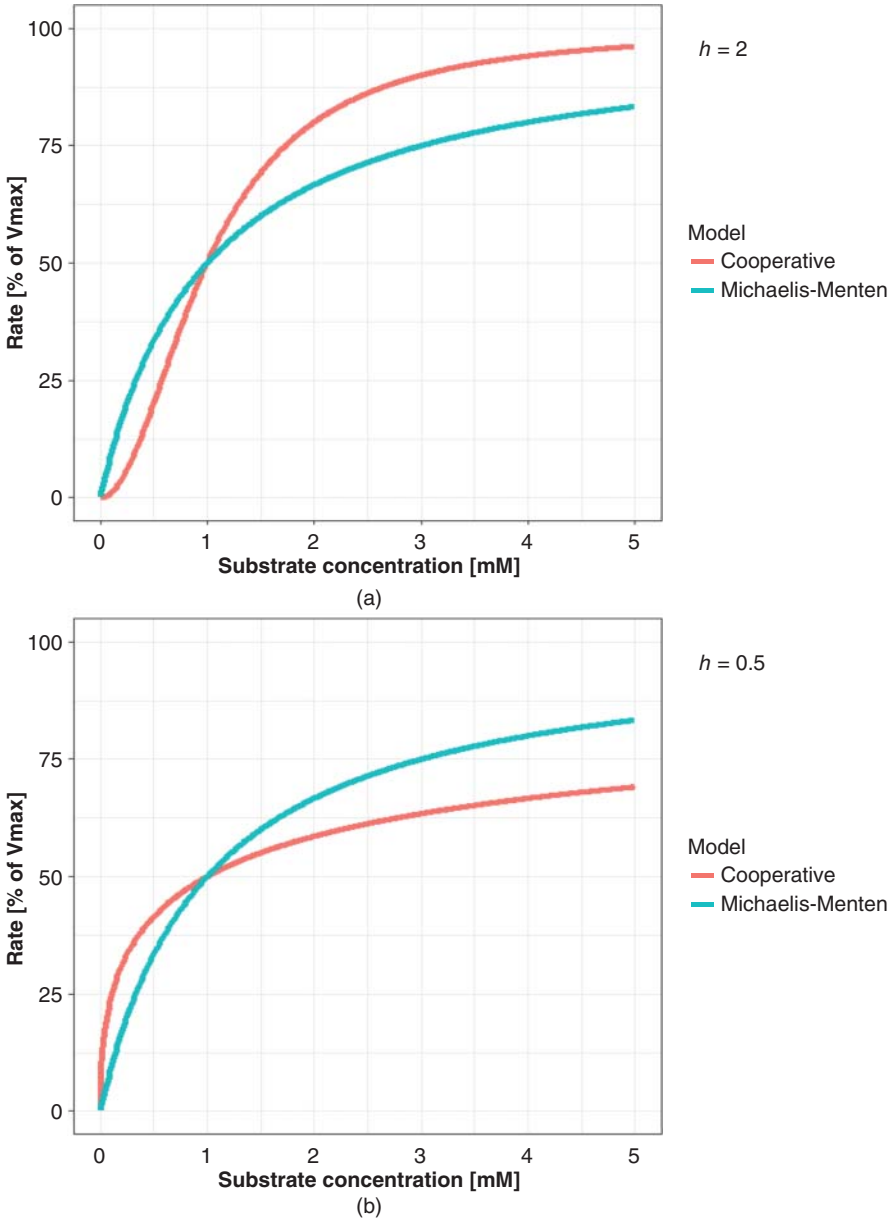

Figure 9.6 Cooperative enzymes. Figures show cooperative kinetics (red), compared to Michaelis–Menten kinetics (blue). The compared kinetics have $K_M/K_{½} = 1$ mM. (a) Positive cooperativity ($h = 2$). The rate at low substrate concentrations is considerably lower than the Michaelis–Menten case. (b) Negative cooperativity ($h = 0.5$). The approach to saturation is considerably slower than the Michaelis–Menten model.

9.2.2.2 Multiple Substrates

Enzymes that have more than one substrate – the majority of enzymes – also deviate from Michaelis–Menten kinetics. With multiple substrates (and usually multiple products), the reaction schemes become more complicated (Figure 9.7). Each addition to the reaction will result in extra kinetic steps that must be modelled. Even in the simplest case (sequential bisubstrate enzyme – e.g. benzaldehyde lyase [34, 35]), this results in two extra

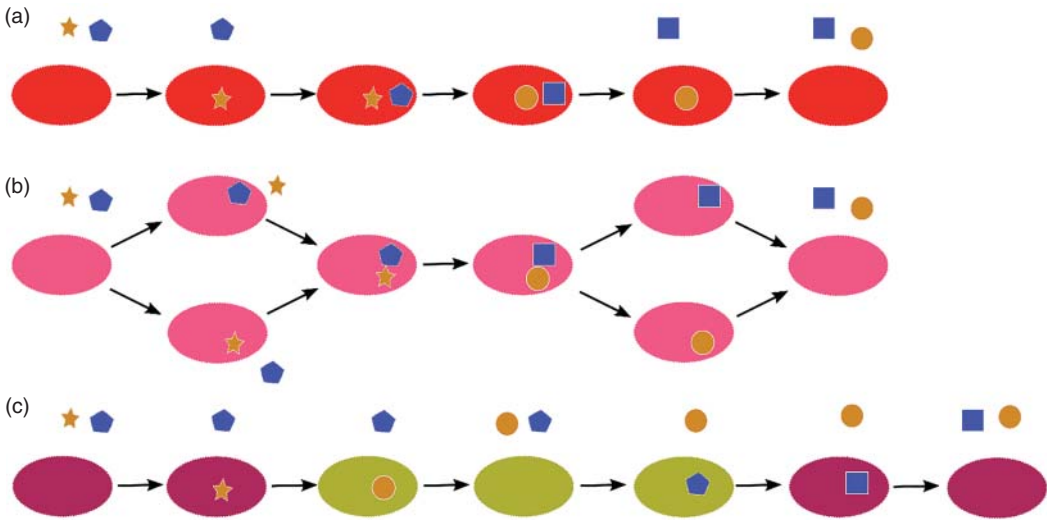

Figure 9.7 Bisubstrate reaction mechanisms. Approximately 60% of enzymes have two substrates and two products. The substrates and products bind and release in three main schemes. Enzymes are shown as red/pink/maroon/green ovals; substrates as yellow stars/blue pentagons; products as yellow circles/blue squares. (a) Ordered sequential bisubstrate mechanism. One substrate (yellow) must bind before the second (blue). After reaction, the product corresponding to the second substrate to bind is released first. (b) Random sequential bisubstrate mechanism. Either substrate can bind to the enzyme first; after the reaction, either product can be released first. (c) 'Ping-pong' mechanism. One substrate will bind to the enzyme, and react, producing one product and a modified enzyme (green). After the first product is released, the second substrate binds. This then reacts to form the second product, with the enzyme returned to its original state.

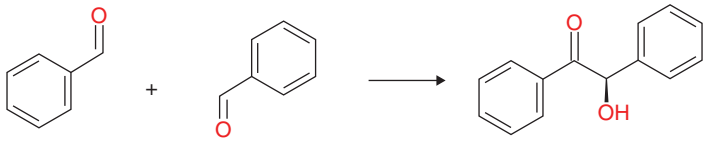

(a)

$$E + 2S \underset{k_{-1a}}{\overset{k_{1a}}{\rightleftharpoons}} ES + S \underset{k_{-1b}}{\overset{k_{1b}}{\rightleftharpoons}} ES_2 \xrightarrow{k_2} EP \longrightarrow E + P$$

(b)

Figure 9.8 Forward reaction for a simple bisubstrate enzyme. The enzyme benzaldehyde lyase [34, 35] combines two molecules of benzaldehyde to form the product *R*-benzoin (a). As the two substrates are identical, the kinetics are simpler. Nevertheless, there are two additional rate constants in the reaction (b).

kinetic constants (Figure 9.8). Many of these more complicated schemes can also be simplified using similar assumptions to those in the Michaelis–Menten equation, and the steady-state approximation. For example, in the case of the sequential bisubstrate reaction (Figure 9.8), the corresponding rate equation is [21, 22]

$$v = \frac{V_{max}[A][B]}{K_i^A K_M^B + K_M^B[A] + K_M^A[B] + [A][B]}. \tag{9.12}$$

This equation describes the general case for a steady-state ordered mechanism [21]. In cases where the formation of the EA complex is in equilibrium (i.e. $k_{-1a} \gg k_2$; equilibrium ordered mechanism), the $K_M{}^A[B]$ in the denominator is removed.

It should be clear from this rate equation that it is considerably more challenging to determine all of the necessary parameters. The equation now contains four parameters (V_{max}, $K_M{}^A$, $K_M{}^B$ and $K_i{}^A$) and two variables (for the two substrate concentrations). A general approach is to set the concentration of one substrate to a high (saturating) level, where the substrate concentration is expected to be well in excess of K_M (and so the $[S]/(K_M + [S])$ term for that substrate approximates to 1). The *apparent* K_M ($K_{M\,app}$) of the other substrate in these conditions can then be determined. This K_M will be an amalgam of the true K_M for this substrate and the $K_i{}^A K_M{}^B$ term. The *case study* demonstrates the determination of these apparent K_M values for an example substrate. A more involved experiment allows the accurate determination of all four parameters (see *protocol*).

Enzymes that have more than two substrates can also be investigated using similar schemes. As the number of substrates increases, so does the number of parameters and consequently it becomes increasingly important to have a clear understanding of the likely reaction mechanism. The same caveats regarding the Michaelis–Menten equation apply even more so in these more complicated mechanisms. This is so particularly for the effects of product inhibition, as the greater number of products make it likely that this will be significant considerably earlier in the reaction.

9.3 Determination of Enzyme Kinetic Mechanisms

9.3.1 Michaelis–Menten Parameters

Investigation of the Michaelis–Menten parameters of a newly isolated enzyme for a presumed substrate is generally an incremental process. The design of a well-designed enzyme assay is discussed in detail in key textbooks [19, 21]. Once this is available, obtaining reliable, high quality data will take several scouting experiments to obtain the right conditions. Acquiring data at the right enzyme and substrate concentrations is essential to determine the kinetic parameters with high confidence. This is particularly important when attempting to differentiate between mechanisms.

The first prerequisite is to determine an appropriate concentration of enzyme to use. An ideal enzyme concentration will allow an accurate determination of the rate (ideally while the first 10% of substrate is consumed) at high substrate concentrations. This is essential for an accurate determination of V_{max}. However, the enzyme concentration used should also permit determination of the reaction rate when this rate is 5–10% of the high substrate case. This is important for collecting data at substrate concentrations well below K_M, and so for an accurate determination of K_M, and also for identifying positively cooperative enzymes (which are typically identified by unexpectedly low rates at low substrate concentrations). These criteria are generally easier to achieve with continuous, rather than stopped, assays [19, 21]. It is important in when designing this experiment to consider the effects of the enzyme's buffers and carriers (especially glycerol) on the reaction when determining the highest practical concentration. Experiments should include a no enzyme control, to account for non-enzymatic changes in the signal (e.g. natural slow breakdown of NADH at 37 °C). An example of a refined experiment is shown in Figure 9.9. Note that the units for enzyme reactions are conventionally given as units of time and concentration (ideally k_{cat} in per second and K_M in mM or μM). Extensive recommendations are available at https://www.beilstein-strenda-db.org/strenda/public/guidelines.xhtml [36].

Ideal features from a refined experiment would show:

- A graph of enzyme concentration against rate (Figure 9.9b) shows that at the enzyme concentration selected, the rate of reaction is proportional to the enzyme concentration.
- The reaction rate can be accurately measured, ideally in the first 10% of substrate usage, for the selected enzyme concentration (i.e. for a continuous assay, a linear section of at least five points can be measured; for a stopped assay, the rate of reaction is consistent over at least two of the time periods tested).
- An accurate measurement could be taken with the rate at 5–10% of the observed rate at the enzyme concentration selected.

Examples where these criteria would not be met are shown in Figure 9.10. In many cases, it may not be possible to fulfil all of these criteria for a given enzyme reaction. In this case, the experimenter must select

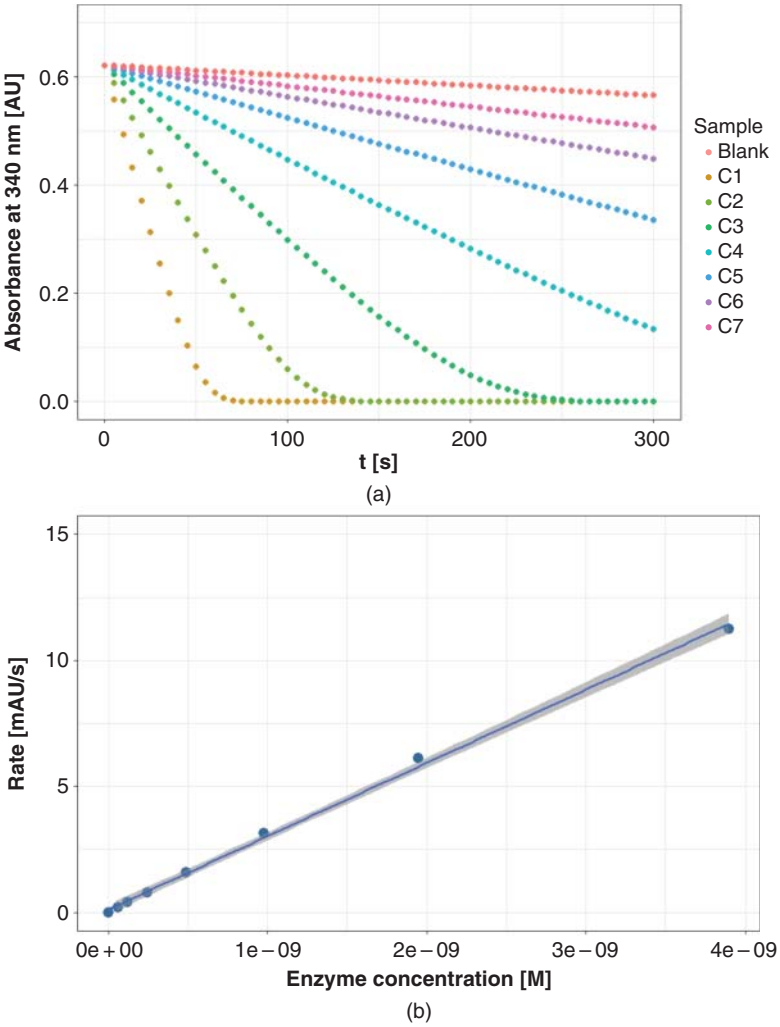

Figure 9.9 Example of an optimised experiment to determine ideal enzyme concentrations. Data are modelled for lactate dehydrogenase from rabbit muscle, using the reverse reaction: pyruvate + NADH → lactate + NAD^+. The reaction is modelled as irreversible. Kinetic parameters: $K_M^{pyruvate} = 150$ µM; $K_M^{NADH} = 12$ µM; $K_i^{pyruvate} = 75$ µM; $k_{cat} = 6.7 \times 10^8$ per second; background rate of NADH degradation 0.03 µM/s. The model uses a volume of 200 µL, with initial concentrations of 1 mM pyruvate, 100 µM NADH. Enzyme is modelled at seven concentrations, with a maximum concentration of 3.9 nM (equivalent to ~0.03 unit in 200 µL – C1), with twofold dilutions between the concentrations to a minimum of 61 pM (C7). A control with no enzyme is used to determine the background rate (Blank). NADH concentrations are converted to the absorbance at 340 nm (AU: absorbance unit) that would be detected using the extinction coefficient $\varepsilon = 6220$ 1/M/cm. Data are shown for every five seconds, corresponding to detection with a good plate reader. (a) High concentrations of the enzyme (C1, C2) lead to the reaction consuming over 20% of the substrate before many data points can be collected and so would not be appropriate concentrations (especially as fewer data can be collected when using more samples). Concentrations C4 and C5 consume approximately 10–20% of the substrate in 100 seconds and are clearly still within the linear phase: these would allow good data analysis when the substrate concentrations and rate are lower in later experiments. Concentrations C6 and especially C7 show a detectable rate, but when the substrate concentrations are reduced, the rate may not be distinguishable from background. This might result in cooperative behaviour being missed or incorrectly modelled. (b) The rate of reaction is plotted against enzyme concentration. The rate of reaction is linearly related to the enzyme concentration, indicating that enzyme is limiting across this concentration range (note that the highest enzyme concentration shows a slightly lower rate than predicted).

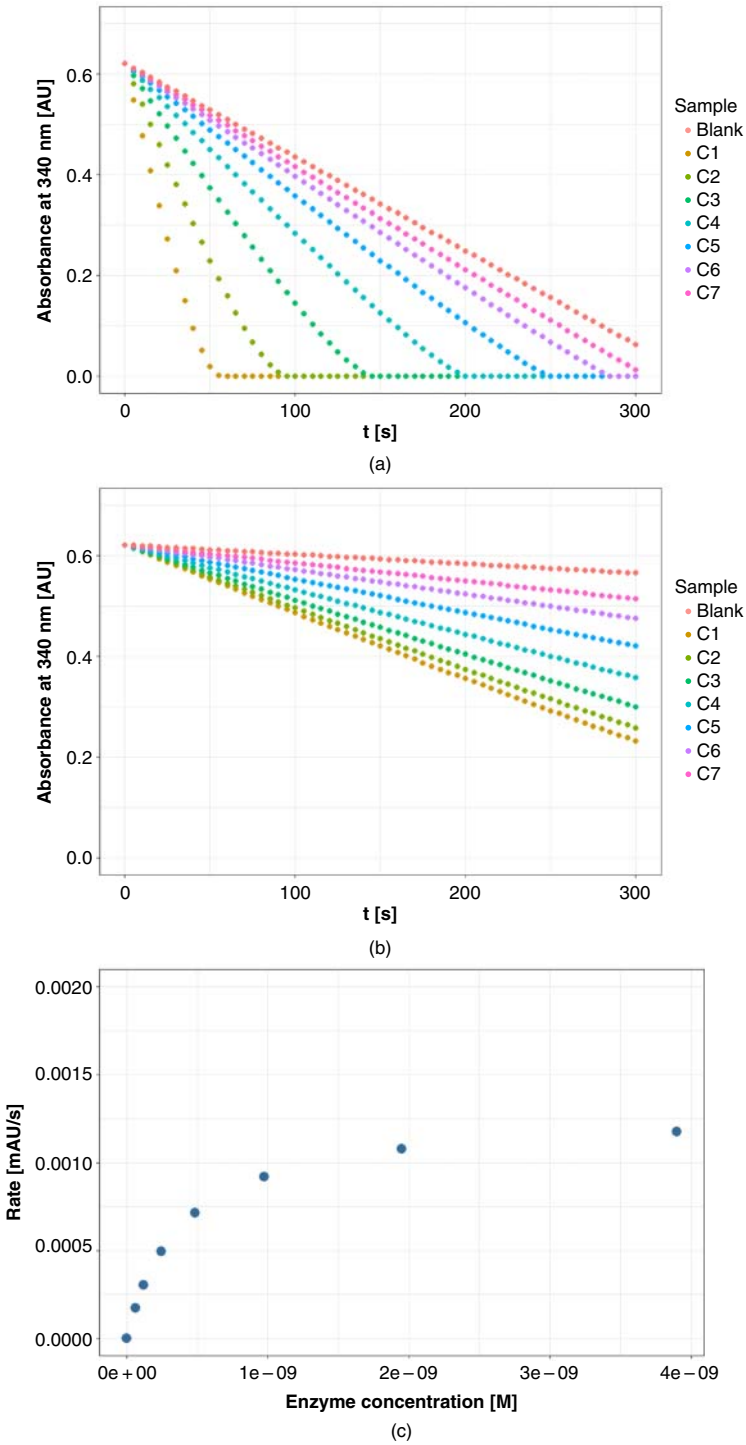

Figure 9.10 Examples of challenging data. (a) Reaction rate is similar to background rate. Here, it will be necessary to use a higher enzyme concentration and continue the reaction until more substrate is exhausted. (b) Enzyme is not limiting at test concentrations. Here the conditions of the reaction make the enzyme no longer the sole determinant of rate. The graph of rate versus enzyme concentration (*C*) does not follow a straight line. Enzyme concentrations at the lower end of the concentration range will have to be used. This may make data collection challenging as the observed rates will be small. A compromise concentration, where the enzyme is still just limiting (most likely around C5) but the rate is still sufficiently above background will have to be chosen.

which criterion to compromise. Making this choice will require consideration of the scientific goals of the enzyme assay.

Once the enzyme concentration has been established, the next stage in determining the kinetic parameters for a monosubstrate enzyme is to obtain a broad estimate of K_M. After the data have been collected (see the detailed protocol below), they are fitted to the Michaelis–Menten equation using a statistical software package. Examples of such packages are *R* (conveniently implemented using RStudio), Graphpad, KaleidaGraph and SPSS. Although linear transformations such as the *Lineweaver-Burk plot* (an example is shown in Figure 9.15) were used before such packages were available, they can amplify errors considerably and should not be used [37]. This will generally provide one of the following outcomes:

- The data fit reasonably well to the Michaelis–Menten equation, with the estimated K_M well within the range of substrate concentrations tested. In this case it is appropriate to move to more detailed investigations.
- The data appear to follow a straight line passing through the origin. This indicates that the data do not cover values above K_M sufficiently well. This generally indicates that the substrate is not an ideal substrate for this enzyme. This is often observed in situations where the initial substrate concentration has been selected based on a homologue and the enzyme studied does not prefer this substrate. If it is possible to increase the highest substrate concentration, repeat the experiment starting with the highest practicable concentration. In cases where a saturating substrate concentration cannot be reached, it is possible to determine k_{cat}/K_M (e.g. see [38, 39]).
- The enzyme shows a high, similar rate in all conditions. This indicates that the substrate range is all above K_M. In this case, the experiment should be repeated, starting at one of the lower substrate concentrations and using fourfold dilutions.
- The data fit poorly to the Michaelis–Menten equation. There are several ways in which this might be the case. In this situation, it is best to fit the data to a model for cooperativity (Eq. (9.11)) or substrate inhibition (Eq. (9.13)) as appropriate. The estimated parameters should be used to perform a more detailed experiment, using the wider substrate range discussed. This detailed experiment must be undertaken with the expectation that the data analysis will require one of the more complicated scenarios discussed later.

Examples of an initial substrate range determination in these scenarios is shown in Figure 9.11.

Once an estimate of K_M has been determined in this manner, more detailed experiments should be performed. It is highly important to have a good range of substrate concentrations both above and below K_M. Substrate concentrations considerably in excess of K_M are necessary to obtain a good estimate of V_{max}. This is essential not only as V_{max} is one of the two parameters to be fitted but also as the K_M value is highly dependent on V_{max} (as, by definition, it is the substrate concentration with a half-maximal rate). Substrate concentrations below K_M are also essential, as these are required to obtain a good estimate of K_M. These low substrate concentration points are also important for identifying cooperative enzymes: substantial deviation from the Michaelis–Menten model in these low substrate concentration points is the best indicator of cooperativity. Therefore, even though these data can be more challenging to obtain accurately, they offer considerable value in understanding the enzyme. These data should be distributed geometrically around K_M – that is, each substrate concentration should be an *n*-fold dilution of the previous substrate concentration. Although arithmetic distributions (i.e. 0.25×, 0.5×, 0.75×, 1×, 1.25×, 1.5×, 1.75× K_M) are superficially more attractive, these will give little information if the estimate of K_M is inaccurate. Once these data have been obtained, they should again be fitted to the Michaelis–Menten equation, as illustrated above.

Examples of such a refinement experiment is shown in Figure 9.12. Likely outcomes from these experiments are:

- The data show a good fit to the Michaelis–Menten equation, with the determined K_M well within the concentrations tested (at least three non-zero data points above and below K_M; Figure 9.12b). In this case, the result may be sufficient for the experimental requirements. If a more accurate determination of the kinetic parameters is required, the experiment should be further refined, as discussed below.

- The data fit reasonably well to the Michaelis–Menten equation, but the refined value of K_M has altered by at least twofold from the initial estimate (Figure 9.12c). In this case, a further refinement of the experiment will be required, as discussed below.
- The data show significant deviations from the Michaelis–Menten equation (Figures 9.12d to f). In these cases, alternative experimental treatments are required. These are detailed in the following sections.

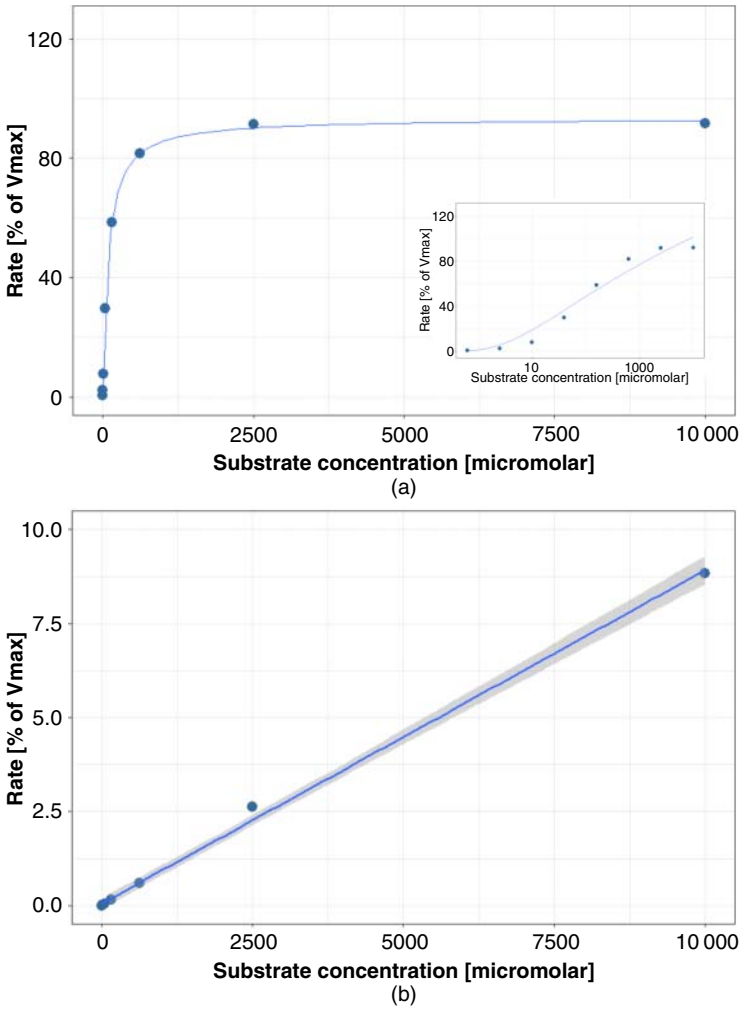

Figure 9.11 Examples of results from an initial substrate concentration experiment. All figures show simulated data, with random errors added for verisimilitude. (a) Effective determination of an estimate of K_M. The data fit well to the Michaelis–Menten equation, with points distributed well above and below the estimated K_M (~100 μM). The inset shows the *x*-axis on a log scale, to highlight the fact that the fit at low concentrations is good. (b) Substrate concentrations used are too low. The data fit best to a straight line, indicating that the substrate concentration is not yet approaching K_M. Higher substrate concentrations would be required in this instance. (c) Substrate concentrations used are too high. Almost all of the substrate concentrations are above K_M, leading to a poor estimate of K_M. This is made clearer using a log scale for the *x*-axis (inset). A repeated experiment, starting at a lower substrate concentration (likely removing the top three concentrations) would be necessary. (d) Results are not monotonic (here substrate inhibition is modelled). The data consequently are a poor fit to the Michaelis–Menten equation. The data should be fitted to the substrate inhibition model. Follow-up experiments would require more data to model the additional parameters required.

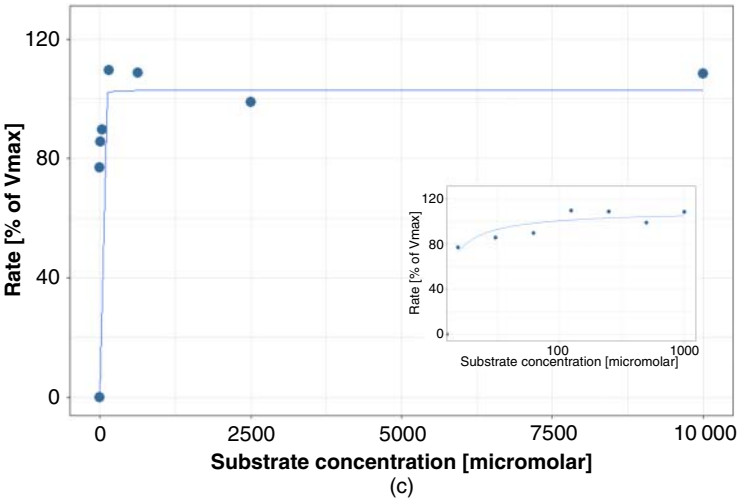

(c)

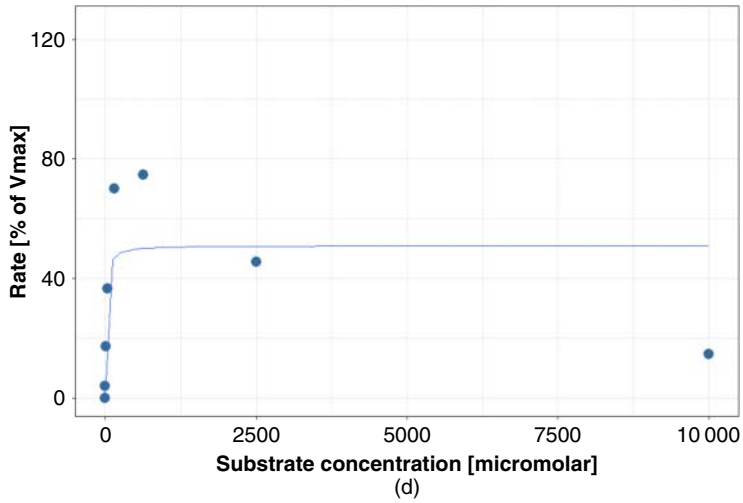

(d)

Figure 9.11 (*Continued*)

Where the experiment requires further more refinement, it is often sensible to collect more data points. Where the data are not determined sufficiently accurately, the next step would be to look for accuracy improvements in the enzyme assay.

9.3.2 Cooperative Enzymes

When the data for a refined enzyme assay remain monotonic (i.e. as substrate concentration increases, the rate always increases), but show deviations from the Michaelis–Menten equation, the most likely explanation is that the enzyme is showing cooperative behaviour (Figure 9.12d and e). Firstly, fit the data to a cooperative model rather than the Michaelis–Menten equation (Figure 9.13). This will provide estimates of the kinetic parameters V_{max}, $K_{½}$[2] and h for the reaction. These parameters will likely be poorly determined as there are

2 For cooperative enzymes, the parameter $K_{½}$ is used rather than K_M. The $K_{½}$ is the substrate concentration where the enzyme activity is 50% of maximum. $K_{½}$ is used to reflect that this parameter will be raised to a power in the cooperative equation.

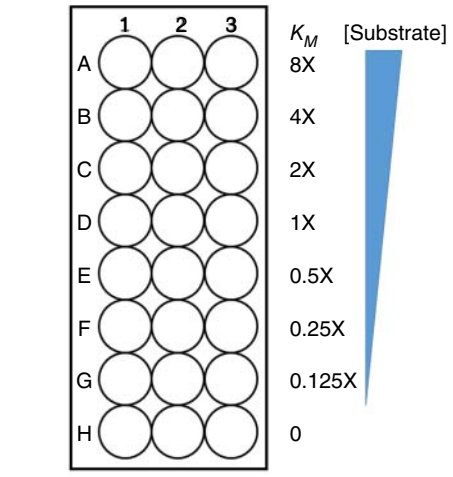

(a)

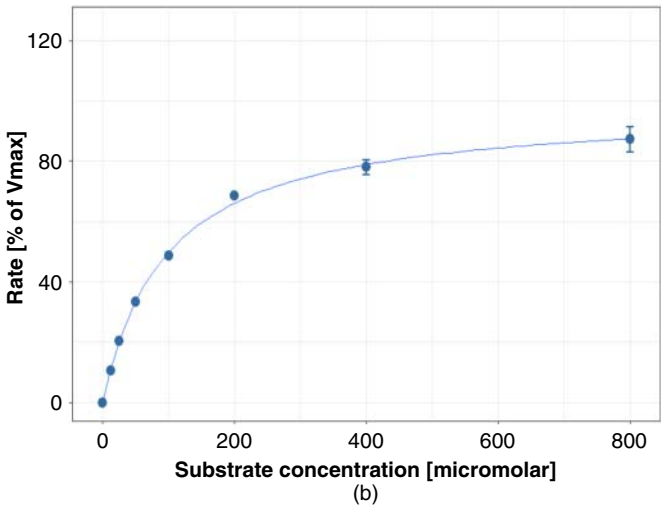

(b)

Figure 9.12 Experimental determination of refined estimates of V_{max} and K_M. Examples are simulated as triplicate experiments with random errors added (normal distribution, SD = 5%) for verisimilitude. (a) Example plate layout for detailed experiment. (b) Example of a successful experiment (expected $V_{max} = 100\%$, $K_M = 100$ μM). The data obtained give $V_{max} = 98 \pm 2\%$, $K_M = 96 \pm 6$ μM. Errors in K_M of less than 10% of the observed value indicate an accurate experiment. (c) Example of an experiment where the estimated K_M was inaccurate (expected $V_{max} = 100\%$, $K_M = 500$ μM). The data obtained give $V_{max} = 100 \pm 3\%$, $K_M = 500 \pm 30$ μM. Although the values obtained are accurate, with only one data point at a substrate concentration above K_M this cannot be trusted. (d) Example of a positively cooperative enzyme (expected $V_{max} = 100\%$, $K_M = 100$ μM, $h = 2$). The data fit poorly to the Michaelis–Menten equation (red line; observed $V_{max} = 125 \pm 7\%$, $K_M = 170 \pm 30$ μM), but fit well to the cooperative enzyme equation (Eq. (9.11); blue line; observed $V_{max} = 98 \pm 2\%$, $K_{½} = 98 \pm 3$ μM, $h = 1.9 \pm 0.1$). Note that the major deviation is at a low substrate concentration. (e) Example of a negatively cooperative enzyme (expected $V_{max} = 100\%$, $K_M = 100$ μM, $h = 0.5$). The data fit poorly to the Michaelis–Menten equation (red line; observed $V_{max} = 71 \pm 2\%$, $K_M = 30 \pm 3$ μM), but fit better to the cooperative enzyme equation (blue line; observed $V_{max} = 100 \pm 10\%$, $K_{½} = 90 \pm 50$ μM, $h = 0.50 \pm 0.06$). Note that there are deviations from Michaelis–Menten at a low substrate concentration, and also at high concentrations. (f) Example of substrate inhibition (expected $V_{max} = 100\%$, $K_M = 100$ μM, $K_i = 400$ μM). The data fit poorly to the Michaelis–Menten equation (red line; observed $V_{max} = 41 \pm 2\%$, $K_M = 21 \pm 6$ μM), but fit clearly better to the substrate inhibition equation (Eq. (9.13); blue line; observed $V_{max} = 90 \pm 10\%$, $K_M = 80 \pm 20$ μM, $K_i = 500 \pm 100$ μM). Note that there are deviations from Michaelis–Menten at high substrate concentrations, but at low concentrations the fit is reasonable.

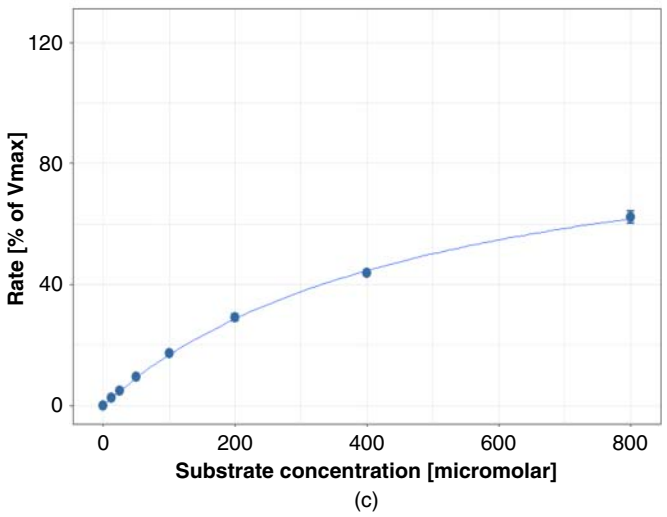

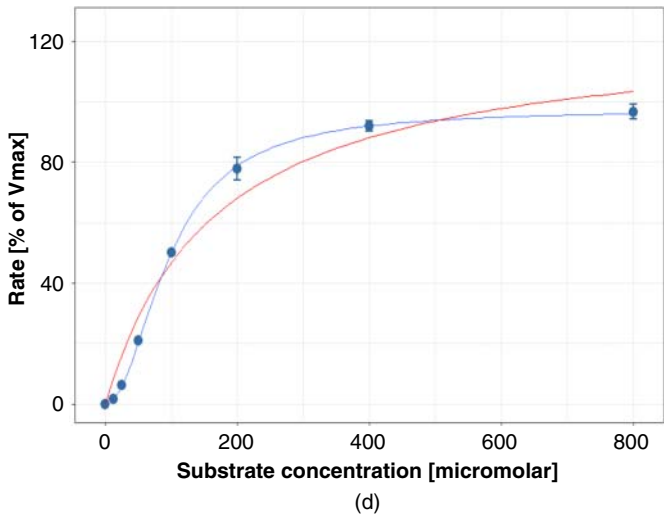

Figure 9.12 (*Continued*)

insufficient data to fit so many parameters. A following experiment should be performed using a larger number of data points (12–16) and refined substrate concentrations. For positively cooperative enzymes, collecting data up to 5× $K_{½}$ is sufficient. With positive cooperativity, the reaction approaches V_{max} more rapidly than for a Michaelis–Menten enzyme and so a tight focus around $K_{½}$ is most appropriate. For negatively cooperative enzymes, a wider range (up to 10× or even 20× $K_{½}$) is appropriate. Negatively cooperative enzymes approach V_{max} at much higher substrate concentrations than Michaelis–Menten enzymes and show low rates only at quite low multiples of $K_{½}$. As described below, these data should be distributed geometrically around $K_{½}$. These experiments should provide an accurate determination of the kinetic parameters. As discussed in the case of Michaelis–Menten enzymes, if there is a desire to determine the parameters more accurately, more data points can be obtained; however, it is also likely that the biggest improvements in data quality will come from improving the enzyme assay itself.

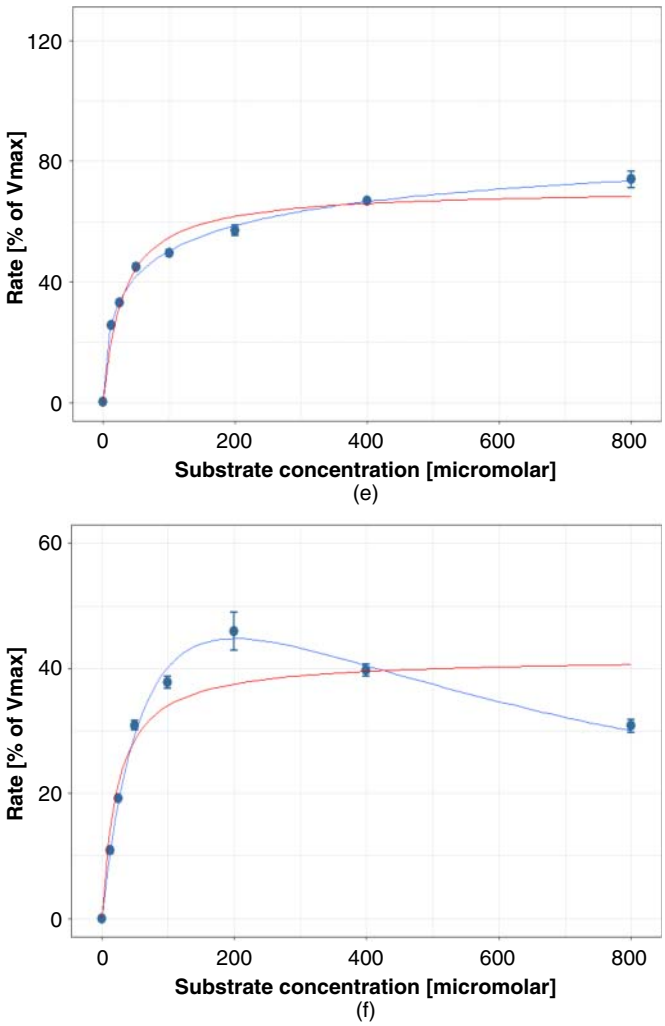

Figure 9.12 (*Continued*)

9.3.3 Substrate Inhibition

Approximately 20% of enzymes show inhibition by their own substrates [40]. This often occurs in enzymes with at least two substrates, where one substrate can bind to site that the second substrate should occupy in addition to the catalytic binding site; alternatively, the substrate can bind at an allosteric site. Enzymes that display substrate inhibition show a classical effect where, above a certain substrate concentration, the rate of reaction starts to fall in an approximately hyperbolic fashion (Figure 9.14a). The Michaelis–Menten equation is modified by an additional term that causes the K_M to inflate with increasing substrate concentration as the *inhibition constant* K_i is approached and exceeded [41]:

$$v = \frac{V_{\max}[S]}{K_M + \left([S]\left(1 + \frac{[S]}{K_i}\right)\right)}, \tag{9.13}$$

where v is the initial reaction rate, V_{max} is the reaction rate at infinite substrate concentration, $[S]$ is the substrate concentration, K_M is the Michaelis constant and K_i is the substrate inhibition constant.

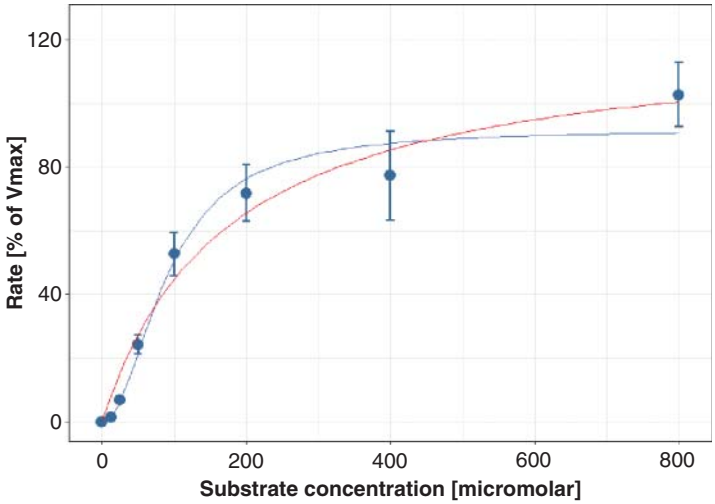

Figure 9.13 Example of a cooperative enzyme with significant errors. Example is simulated as triplicate experiments (expected $V_{max} = 100\%$, $K_{½} = 100$ µM, $h = 2$) with random errors added (normal distribution, SD = 20%). The data fit poorly to the Michaelis–Menten equation (red line; observed $V_{max} = 120 \pm 10\%$, $K_M = 170 \pm 50$ µM), but fit well to the cooperative enzyme equation (Eq. (9.11); blue line; observed $V_{max} = 100 \pm 10\%$, $K_{½} = 110 \pm 30$ µM, $h = 1.4 \pm 0.4$).

Where substrate inhibition is detected or suspected, experiments should be performed with a minimum of 12 data points in triplicate (including a negative control). These should be distributed to have at least three substrate concentrations below the lower of K_M and K_i (ideally reaching at least three times less than the lower of these), at least three substrate concentrations above the greater of K_M and K_i (ideally reaching at least three times greater than the higher of these) and substrate concentrations between the two constants if possible (Figure 9.14b).

9.3.4 Determination of the Mechanism of a Bisubstrate Enzyme

Bisubstrate enzymes adopt three common general mechanisms (random sequential binding, ordered sequential binding and ping-pong mechanisms; Figure 9.7). Distinguishing which of these mechanisms an enzyme adopts, and the order of substrate binding if appropriate, adds a great deal of value to understanding the enzyme. This is particularly the case when the goals of a project require the modulation of enzyme activity (e.g. in a drug development program or when seeking to understand the role of an enzyme *in vivo* using known inhibitors). By selecting the right substrate binding site to target for the enzyme mechanism and the experimental conditions, a stronger effect can be achieved. For example, kinetic analysis of dihydrofolate reductase (DHFR), a target for antimicrobials and anticancer drugs, indicated that release of the tetrahydrofolate product was the limiting step in the reaction [42]. Consequently, drugs that target DHFR generally bind to the substrate/product folate binding site.

The first stage in determining the mechanism is to perform a kinetic parameter determination for one substrate at different concentrations of the second. A Lineweaver–Burk plot of the resulting data will show one of two patterns. Parallel fitted straight lines correspond to a ping-pong mechanism, while fitted lines that meet at a point correspond to sequential bisubstrate models (Figure 9.15). It does not matter which of the two substrates is considered to be the 'first' or 'second' substrate for this experiment: the results are identical regardless of which is chosen (demonstrated in Figure 9.16 from Eqs. (9.12) and (9.14), it should be apparent that the substrates are equivalent in the general cases). For an accurate determination of the correct model, the data should then be fitted to the competing models using suitable statistical software [21, 22]. This will

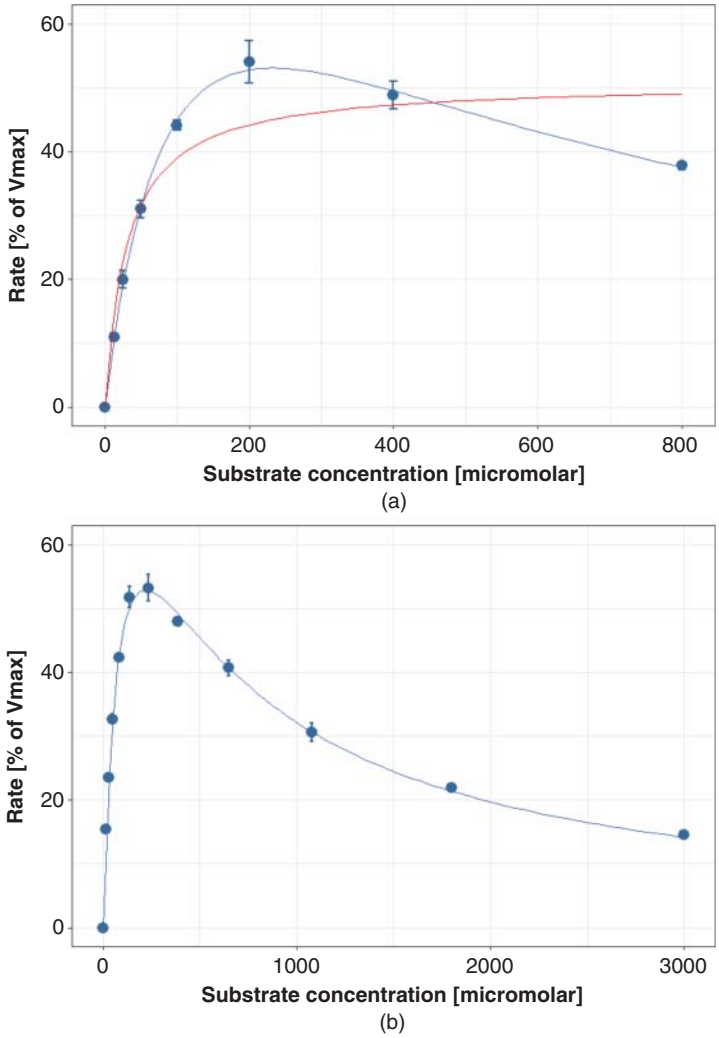

Figure 9.14 Experimental determination of refined estimates of V_{max} and K_M for an enzyme showing substrate inhibition. Examples are simulated as triplicate experiments with random errors added (normal distribution, SD = 5%) for verisimilitude. (a) Example of an initial experiment showing substrate inhibition (expected $V_{max} = 100\%$, $K_M = 100\ \mu M$, $K_i = 500\ \mu M$). The data obtained show a clear deviation from the Michaelis–Menten equation (red line; $V_{max} = 51 \pm 2\%$, $K_M = 30 \pm 7\ \mu M$). Note that the deviation is not readily apparent from the parameter estimates obtained (which might represent a result with high errors and a less accurate initial estimate of K_M) and that it is necessary to examine the graph. The data fit well to Eq. (9.13) (blue line; $V_{max} = 100 \pm 10\%$, $K_M = 110 \pm 20\ \mu M$; $K_i = 500 \pm 100\ \mu M$). Note that while the fitted parameters are a good estimate of the modelled data, they are not obviously more accurate than the Michaelis–Menten equation parameters, as three parameters have been fitted to eight substrate concentrations (underdetermination). (b) A more detailed experiment with 12 data points (here chosen as 0, 18, 30, 50, 84, 140, 233, 389, 648, 1080, 1800, 3000 μM substrate). Accurate estimates are obtained for all three parameters (observed $V_{max} = 99 \pm 4\%$, $K_M = 97 \pm 8\ \mu M$, $K_i = 500 \pm 40\ \mu M$).

also provide accurate determination of all of the kinetic parameters:

$$v = \frac{V_{max}[A][B]}{K_M^B[A] + K_M^A[B] + [A][B]}, \tag{9.14}$$

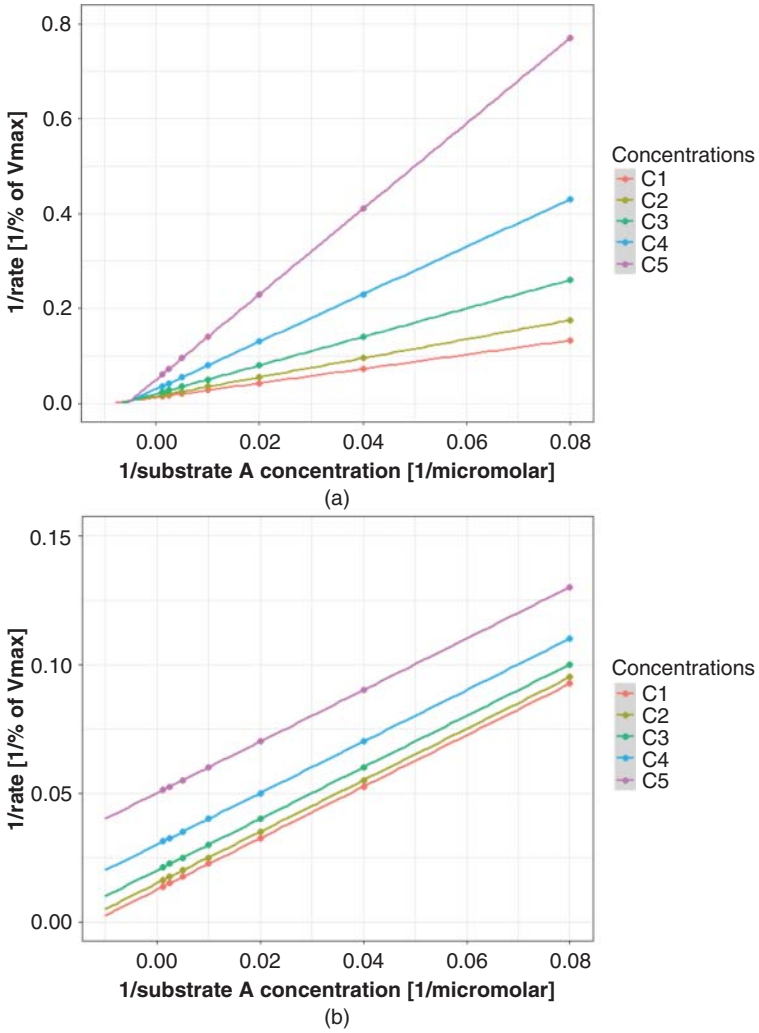

Figure 9.15 Diagnostic experiment to differentiate between kinetic mechanisms of bisubstrate enzymes. Enzymes are modelled with parameters of $V_{max} = 100\%$, $K_M{}^A = 100$ μM, $K_M{}^B = 300$ μM, $K_i{}^A = 200$ μM. In each case, five parallel experiments at different concentrations of substrate B are performed (C1, C2, C3, C4 and C5: 4×, 2×, 1×, 0.5×, 0.25× $K_M{}^B$), testing eight concentrations of A. Lineweaver–Burk plots of perfect data are shown. (a) sequential mechanism; (b) ping-pong mechanism.

$$v = \frac{V_{\max}[A][B]}{K_i^A K_M^B + K_M^B[A] + K_M^A[B] + [A][B]} \tag{9.12}.$$

These equations for testing bisubstrate mechanisms correspond to the sequential and ping-pong mechanisms, respectively.

The quality of fit to the two models can then be compared statistically to determine the likelihood that each model is correct. In this case an appropriate test is the Akaike Information Criterion test [43, 44]. This test uses likelihood-based methods to distinguish which of two (or more) theoretical models are more likely to give the data observed, and is readily implemented by major statistical packages. The experiment should be designed to collect sufficient data to give the desired statistical confidence in the preferred model (Figure 9.17).

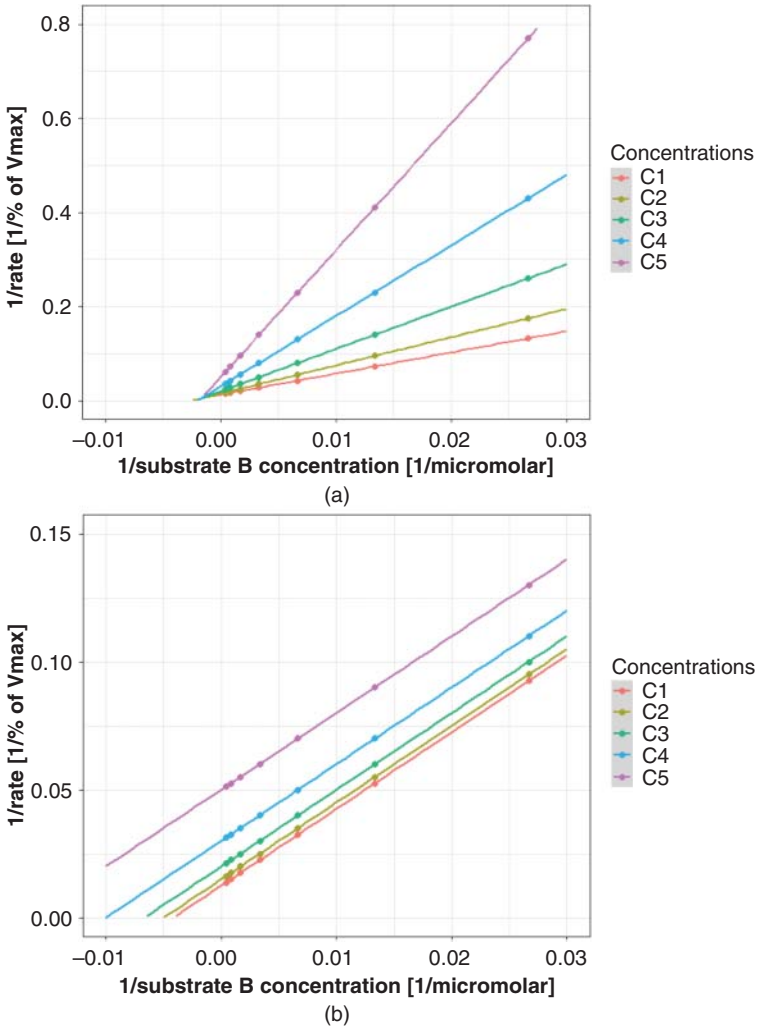

Figure 9.16 The order of substrates selected to differentiate between kinetic mechanisms of bisubstrate enzymes does not matter (cf. Figure 9.15). Enzymes are modelled with parameters of $V_{max} = 100\%$, $K_M{}^A = 100$ µM, $K_M{}^B = 300$ µM, $K_i{}^A = 200$ µM). In each case, five parallel experiments at different concentrations of substrate A are performed (C1, C2, C3, C4 and C5 correspond to 4×, 2×, 1×, 0.5×, 0.25 $K_M{}^A$), each exploring eight concentrations of B. Lineweaver–Burk (double reciprocal) plots of perfect data are shown. (a) Sequential mechanism; (b) ping-pong mechanism.

This experiment can identify a ping-pong mechanism. However, it cannot distinguish between the random equilibrium sequential and ordered sequential mechanisms. To distinguish between these two mechanisms, a detailed product inhibition study must be performed, using each product as the inhibitor with both substrates. The product inhibition equations for the two reactions types are beyond the scope of this chapter (for detail see Chapter 6 of [21] and Chapter 6 of [19]). The experiments should be performed using one substrate at either $K_{M\,app}$ or saturating levels (see Table 9.1) and varying the other substrate above and below $K_{M\,app}$. The products should be tested using at least five product concentrations, ideally covering a little product, the $K_{M\,app}$ of the cognate substrate and the 'saturating' concentration of the cognate substrate (see the *protocol* below). An example of such an experiment is shown in Figure 9.18. The range of useful experiments and the expected outcomes for the different mechanisms are listed in Table 9.1.

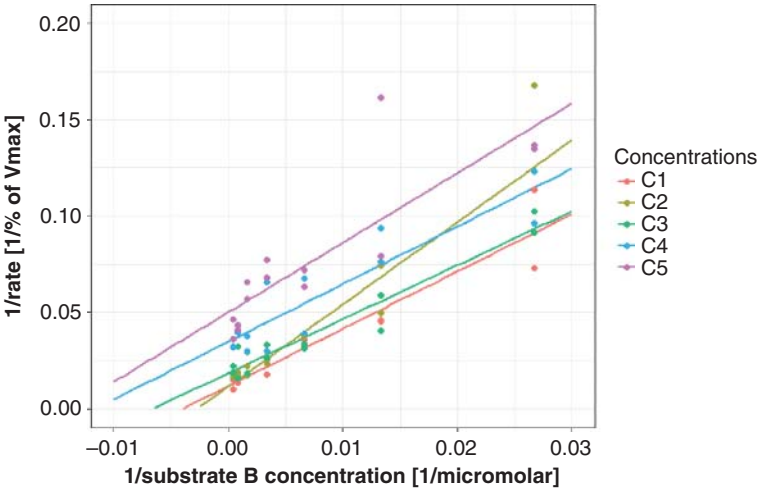

Figure 9.17 Errors in data make interpretation challenging. Data are modelled with the same parameters as Figure 9.16b, but with errors added (normal distributions with SD of 20% proportional error, 10% of V_{max} absolute error) to simulate the increased errors seen at low substrate concentrations. Data are simulated in duplicate: diagnosing the correct mechanism would be challenging.

Table 9.1 Experimental parameters for determining the mechanism of a bisubstrate enzyme using substrate inhibition.

Substrate varied	Product inhibitor used	Constant substrate and concentration	Inhibition pattern		
			Ordered 'steady state'	Ordered equilibrium	Rapid random equilibrium
A	Q	B, K_M^B	Competitive[a)]	Competitive	Competitive
B	Q	A, K_M^A	Non-competitive	Competitive	Competitive[b)]
A	P	B, K_M^B	Non-competitive	No inhibition	Competitive[b)]
A	P	B, 10–50× K_M^B	Uncompetitive	No inhibition	Competitive[c)]
B	P	A, K_M^A	Non-competitive	No inhibition	Competitive

A more detailed description is given in [21], which also provides details for more unusual bisubstrate enzymes.

a) In rare cases where there is isomerisation of the enzyme between states, this can show non-competitive inhibition.

b) Where the product binds only with the other substrate present, this can manifest as other types of inhibition.

c) In cases where only the EBQ complex is a dead-end complex, no inhibition will be seen.

9.4 Technique/Protocol: Determination of Michaelis–Menten Parameters for a Bisubstrate Enzyme and Use of Product Inhibition to Determine Mechanism

All of the experiments shown in this protocol will be illustrated using a model glucose-6-phosphate dehydrogenase enzyme from *Leuconostoc mesenteroides* (Figure 9.19), which can readily be obtained commercially. This enzyme has well-established kinetics and shows an ordered 'steady-state' sequential mechanism [49, 50]. This will be modelled to show no substrate inhibition or cooperativity and product inhibition by NADPH, as has been experimentally established [48]. When analysing the data, these should be considered as discussed above. The enzyme will be considered to have two substrates (*A*: $NADP^+$ and *B*: glucose-6-phosphate) and two products (*P*: 6-phospho-D-glucono-1,5-lactone and *Q*: NADPH).

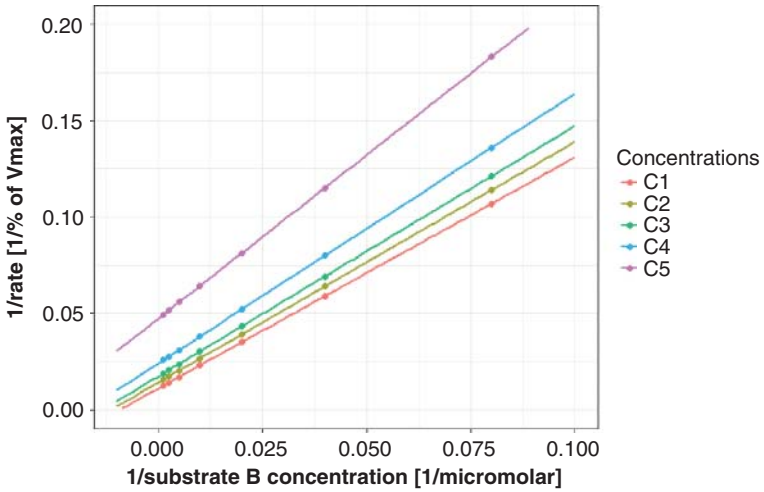

Figure 9.18 Example of a product inhibition experiment. Data are modelled for a steady-state ordered mechanism, using product P as the inhibitor, varying substrate A, with substrate B at 10× K_M. Parameters are as for Figure 9.17b, with K_M and K_i for the products set at double the substrate K_M. The resulting Lineweaver–Burk plot is nearly but not perfectly parallel. Akaike's Information Criterion clearly identifies this as uncompetitive inhibition ($P < 10^{-10}$).

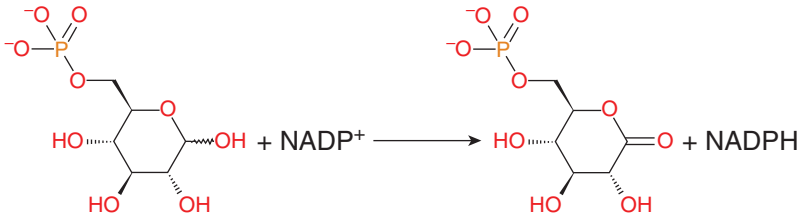

(a)

(b)

Figure 9.19 Glucose-6-phosphate dehydrogenase (G6PD) reaction. (a) Overview of G6PD reaction. (b) Structure of *Leuconostoc mesenteroides* G6PD in complex with glucose-6-phosphate (spheres, carbons white) and $NADP^+$ (spheres, carbons yellow). Figure generated using PyMOL from PDB IDs 1H9A [45] and 1E77 [46] using PyMOL. Approximate kinetic parameters for *L. mesenteroides* G6PD are [47, 48]: K_M^{NADP+}: 5.7 μM, $K_M^{glucose\text{-}6\text{-}phosphate}$: 81 μM, K_I^{NADP+}: 5.07 μM, K_i^{NADPH}: 37.6 μM, k_{cat}: 288 per second.

9.4.1 Method Requirements

- Suitable enzyme assay for determining the initial reaction rate at different substrate and product concentrations.
- Sufficient enzyme and substrates for up to 600 reactions, with each substrate at saturating concentrations.
- Good statistical software (e.g. Graphpad Prism, RStudio, KaleidaGraph, SPSS).

9.4.2 Procedure

9.4.2.1 Determine Suitable Concentrations of the Enzyme to be Used

1. Define an initial estimate of K_M for each component. This should be done using any literature available for substrates A and B with enzymes of the class tested. Where no such literature exists, define K_M as one-tenth of the highest concentration of the relevant substrate that can be practically used.
2. Perform six to eight rate experiments taking single readings with different concentrations of enzyme. Experiments should be performed using substrates A and B at 10× the estimated K_M (step 1). The enzyme concentrations used should start at the highest practical concentration of the enzyme, followed by four- to 10-fold dilutions (depending on the concentrations used and any prior knowledge; where there is no prior knowledge, use 10-fold dilutions). A no enzyme control should be included, using only carrier (Figure 9.20a and b).
3. Plot the rate of the reaction observed in step 2 against the enzyme concentration (Figure 9.20c). The enzyme should be used only in a range where the rate is proportional to the enzyme concentration.
4. Examine the data from step 2. Select a concentration that meets the criteria from step 3: where sufficient data can be obtained to get an accurate rate measurement in the first 10% of substrate use for a continuous assay[3]; where the rate is consistent over at least two time periods when using a stopped assay; and where 5–10% of the observed rate could still be measured above the background level for the reaction.
5. Perform eight rate experiments in triplicate using different concentrations of the enzyme. Perform these at 8×, 4×, 2×, 1×, 0.5×, 0.25× and 0.125× the estimated enzyme concentration determined in step 4, with a no enzyme control (Figure 9.21).
6. Repeat steps 3 and 4 with these more detailed data. Select an enzyme concentration that meets the criteria discussed in these steps as well as possible (Figure 9.9).

9.4.2.2 Determine Estimates of K_M for both Substrates[4]

7. Perform eight rate experiments taking single readings for substrate A. Use the enzyme at the concentration determined in step 6. Use substrate B at 10× the estimated K_M. For substrate A, choose the concentrations based on the quality of the K_M estimate in step 1. Where the K_M was estimated from the literature, perform the experiments with substrate A concentrations of 8×, 4×, 2×, 1×, 0.5×, 0.25× and 0.125× the estimated K_M, with a no substrate control. Where the highest practicable concentration of substrate A is being used, use fourfold dilutions of this (i.e. 1×, 0.25×, 0.0625×, 0.0156×, 0.004×, 0.001× and 0.00025×) with no substrate control (Figure 9.22).
8. Fit these data to the Michaelis–Menten equation using a statistical package. The data will generally show one of the following outcomes (Figure 9.11):
   - The data fit reasonably well to the Michaelis–Menten equation, with the estimated K_M well within the range of substrate concentrations tested. Proceed to step 9.

---

3 In many cases, this can prove impossible to achieve. Increasing this range to 20% of substrate use is still valid (see Figure 9.5), but carries a greater risk of confounding product inhibition effects.

4 When determining the substrate concentrations in these sections, keep in mind that one of the substrates or products will be measured to determine the reaction rate. This may well affect the concentrations of substrate that can be practically used. This may make accurate determination of K_M for one substrate impossible and use of saturating levels of substrate impractical. In this case the $K_{M\,app}$ for the other substrate can be determined at a concentration as close to ideal as is practicable.

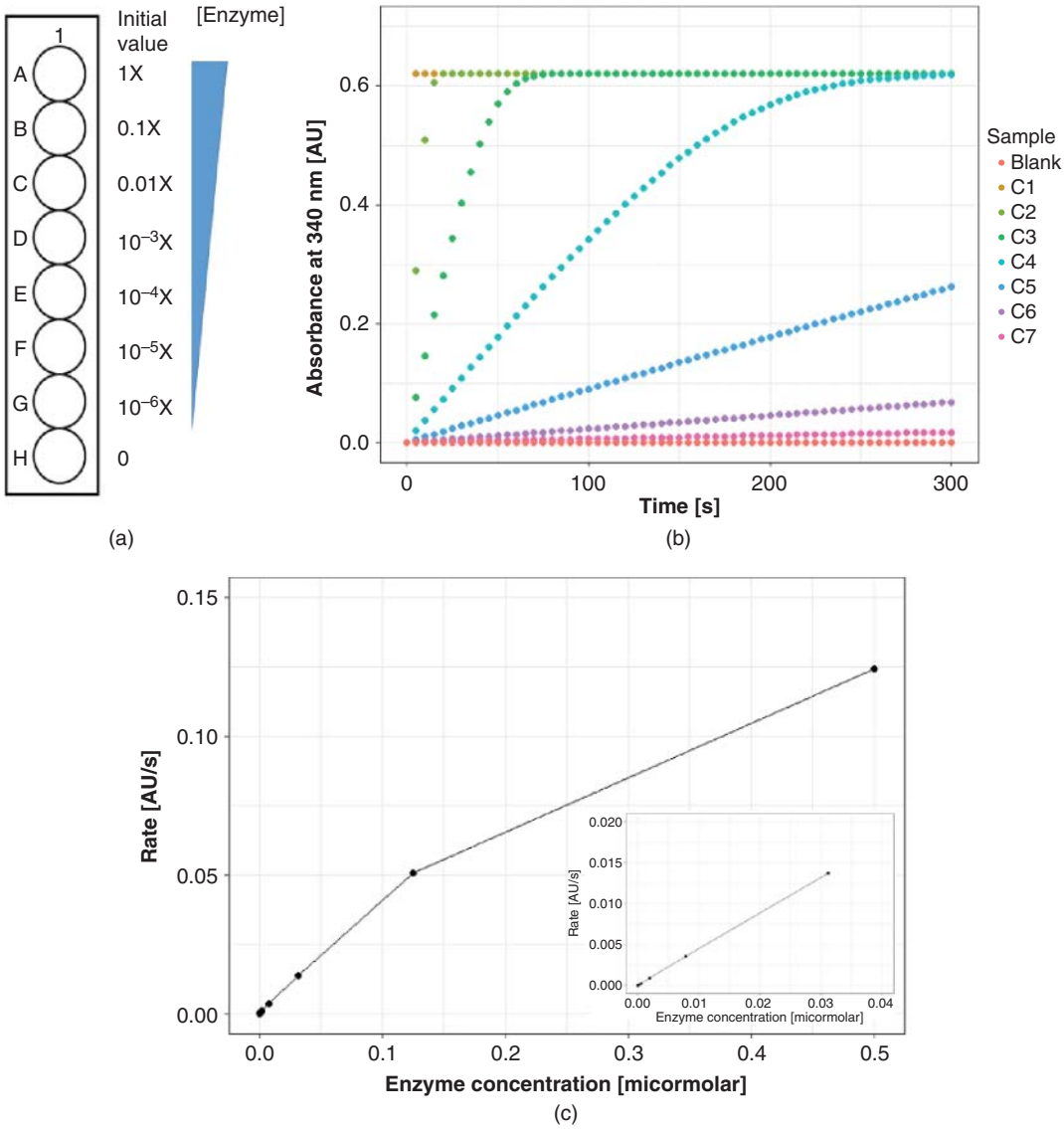

Figure 9.20 Design of the initial experiment to determine enzyme concentration. (a) Plate setup for the experiment where the likely enzyme concentration is unknown. For row A, the highest practical concentration of enzyme should be used. (b) Example with *L. mesenteroides* glucose-6-phosphate dehydrogenase. Here, fourfold dilutions of enzyme are shown from a starting concentration of 500 nM (C1–C7; initial level calculated from the enzyme unit definition). The assay oxidises $NADP^+$ to NADH, which is measured at 340 nm (AU: absorbance unit). (c) Plot of the initial reaction rate against enzyme concentration shows that at high enzyme concentrations, the rate is no longer proportional to enzyme concentration. The inset shows that linearity is maintained up to C3. The data suggest that an enzyme concentration between C4 and C5 would be most appropriate to give enough data to measure and a measureable rate at low substrate concentration.

- The data appear to follow a straight line passing through the origin. If it is possible to increase the concentration of substrate *A*, repeat step 8 with the experiment starting with the highest practicable concentration. Where this has already been done, it will not be possible to determine kinetic parameters for substrate *A*. An alternative is discussed above. Proceed to step 9 for substrate *B*, using the highest practicable concentration of substrate *A*.

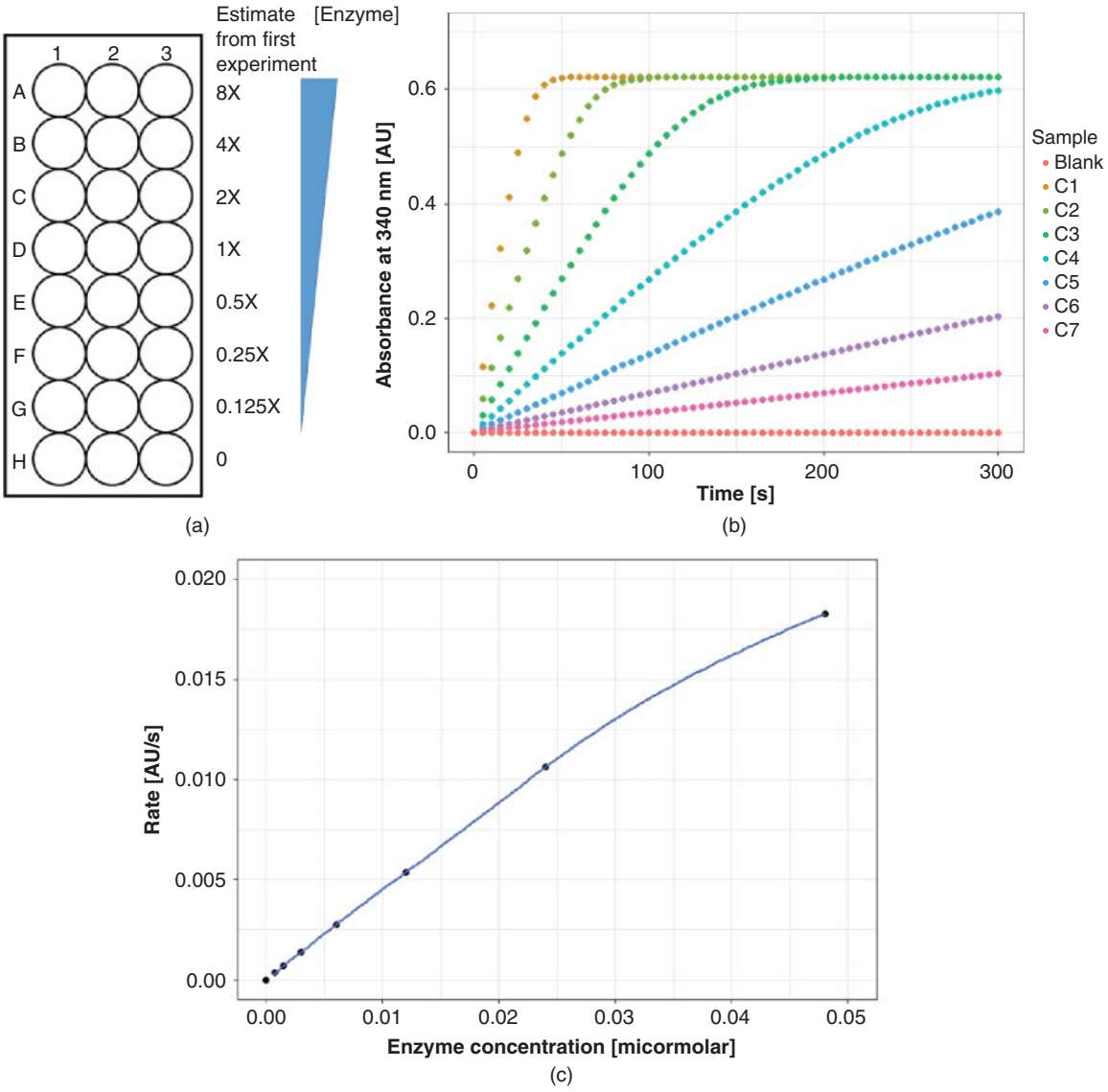

Figure 9.21 Design of the refined experiment to determine enzyme concentration. (a) Plate setup for the experiment, using the result from an initial experiment to guide enzyme concentrations. (b) Example with *L. mesenteroides* glucose-6-phosphate dehydrogenase. Here, twofold dilutions of enzyme are shown from a starting concentration of 48 nM (C1–C7; 48 nM represents 8× the suggested value of 6 nM from Figure 9.20). The assay is designed as in Figure 9.20. (c) Plot of the initial reaction rate against enzyme concentration shows that the high enzyme concentrations start to lose proportionality to enzyme concentration. Here, an enzyme concentration around C4 (6–8 nM) would be most appropriate to give enough data to measure and a measureable rate at low substrate concentration.

- The enzyme shows a high, similar rate in all conditions. Repeat step 8, starting at one of the lower substrate *A* concentrations and using fourfold dilutions.
- The data fit poorly to the Michaelis–Menten equation. Fit the data to an appropriate more complicated equation as described above. Proceed to step 9; the method should be modified as was discussed in the earlier theoretical section according to the scenario that the data correspond to.

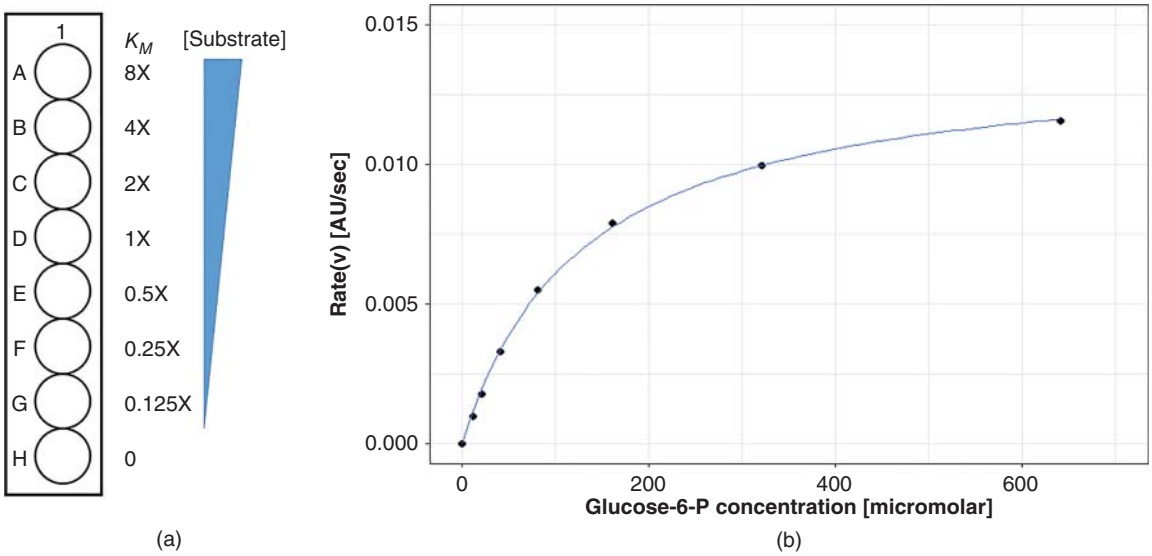

Figure 9.22 Design of the initial experiment to determine the enzyme rate. (a) Plate setup for the experiment, here using literature values to guide substrate concentrations. (b) Example with *L. mesenteroides* glucose-6-phosphate dehydrogenase, varying the concentration of glucose-6-phosphate (AU: absorbance unit). Here, twofold dilutions of substrate are shown from a starting concentration of 640 μM (C1–C7; 640 μM represents 8× the literature value of 81 μM). The model includes random errors in substrate concentrations added and measurements to simulate experimental data. The fit to the Michaelis–Menten equation gives $K_{M\,app}^{G6P}$ of 120 ± 10 μM.

9. Repeat step 7, varying the concentration of substrate *B*. Use a concentration of substrate *A* that is 10× the K_M estimated in step 8. Use the highest practicable concentration of substrate *A* if 10× K_M is greater than this.
10. Repeat step 8 for the analysis of the data collected in step 9.
11. Compare the estimate of K_M for substrate *B* used in step 7 with the refined estimate from step 10. If the refined estimate is no more than twice the original estimate, or the highest practicable concentration of substrate *B* was used, proceed to step 13. Otherwise, repeat the estimate of K_M for substrate *A* as described in step 7, using the refined estimate of K_M for substrate *B* from step 10.
12. Compare the estimate of K_M for substrate *A* used in step 9 with the refined estimate from step 10. If the refined estimate is no more than twice the original estimate or the highest practicable concentration of substrate *A* was used, proceed to step 13. Otherwise, repeat the estimate of K_M for substrate *B* as described in step 9, using the refined estimate of K_M for substrate *A* from step 11. Return to step 11 to consider whether another iteration is required.

9.4.2.3 Determine the Kinetic Parameters for both Substrates Accurately

13. Perform eight[5] rate experiments in triplicate using different concentrations of substrate *A*. Perform these using twofold dilutions from 8× the estimated K_M determined in steps 7–12 (i.e. 8×, 4×, 2×, 1.0×, 0.50×, 0.25X× 0.125× K_M) with a no substrate control. Use a substrate *B* concentration of 10× K_M estimated in steps 7–12, or the highest practicable concentration of this substrate if this is lower (Figure 9.23).
14. Fit these data to the Michaelis–Menten equation using a statistical package. Inspect the output carefully for deviations from the expected shape, especially at low substrate concentrations if these are determined with good confidence.

5 More points, with a subtly different concentration range, may be necessary if the kinetics do not follow the Michaelis–Menten kinetics as discussed above.

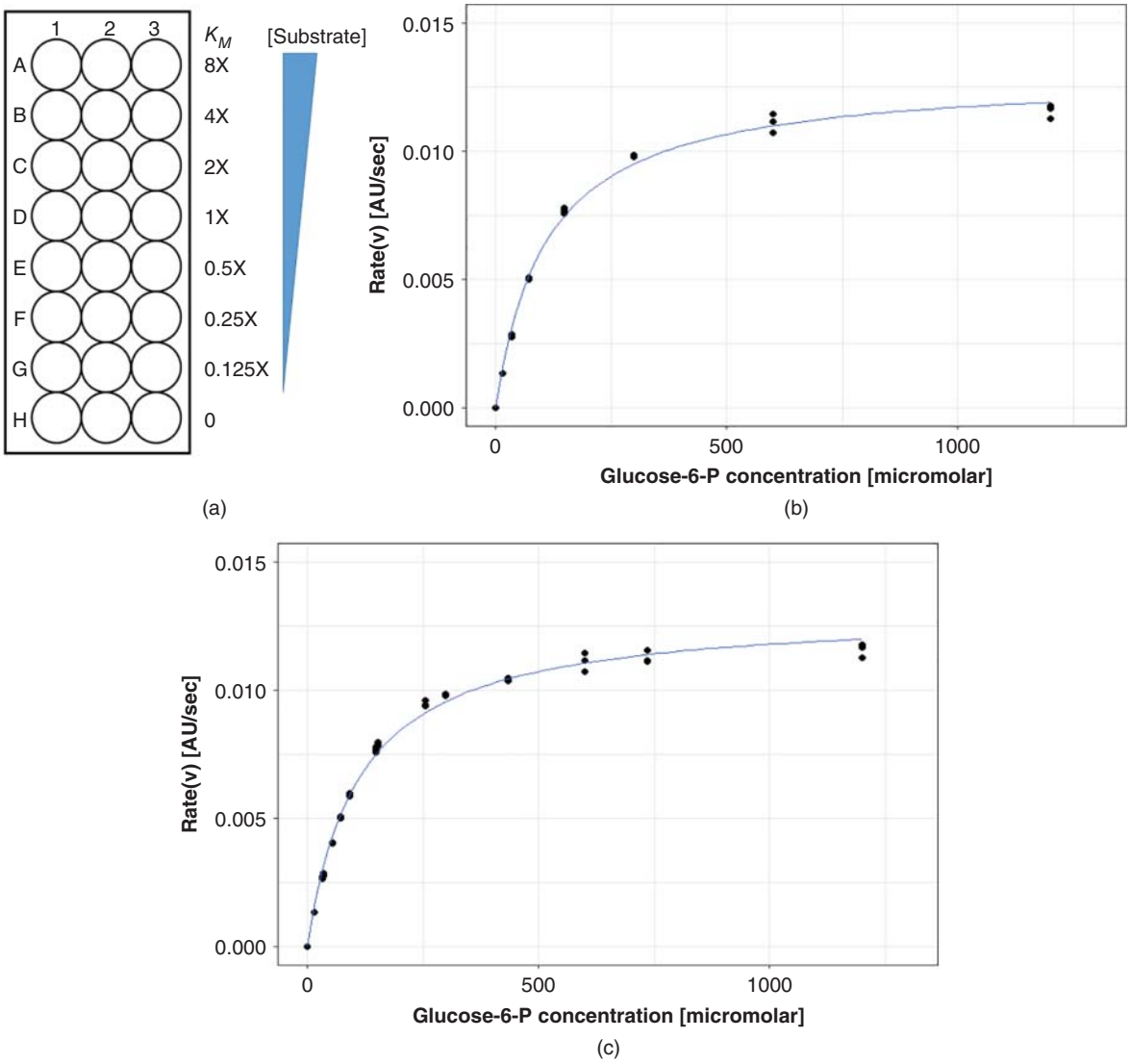

Figure 9.23 Design of refined experiment to determine enzyme kinetic parameters. (a) Plate setup for the experiment, using values from an initial experiment to guide substrate concentrations. (b) Example with *L. mesenteroides* glucose-6-phosphate dehydrogenase, varying the concentration of glucose-6-phosphate. Here, twofold dilutions of substrate are shown from a starting concentration of 1200 μM (C1–C7; 1200 μM represents 8× the estimated value of $K_{M\,app}$ from an initial experiment). The model includes random errors in substrate concentrations added and measurements to simulate experimental data. The fit to the Michaelis–Menten equation gives ${K_{M\,app}}^{G6P} = 110 \pm 5$ μM, $V_{max} = 13.0 \pm 0.02$ mAU/s. (c) Similar simulation to *B*, where additional data using a smaller substrate range for increased accuracy have been added. Addition data use 1.7-fold from a starting concentration of 750 μM (5× the estimated value of $K_{M\,app}$ from an initial experiment). This simulation gives ${K_{M\,app}}^{G6P} = 111 \pm 3$ μM, $V_{max} = 13.1 \pm 0.01$ mAU/s. Note that the errors are reduced. Ten repetitions of these simulations show that the results obtained are typical.

15. Repeat step 13, varying the concentrations of substrate *B*. Use a substrate *A* concentration of 10× K_M estimated in steps 7–12 or the highest practicable concentration of this substrate if this is lower.
16. Fit these data to the Michaelis–Menten equation as in step 14.
17. If the determined values of K_M differ substantially from the estimates used (here – change by at least twofold), repeat steps 13 and/or 15 using the determined K_M as a new estimate. Iterate until the determined values are consistent with the experimental design. Where the determined K_M increased at least twofold, it will be necessary to repeat the experiments to determine the kinetic parameters of the other substrate.
18. If the accuracy of the determined kinetic parameters is sufficient for the experimental need, proceed to step 19. Otherwise, consider the approaches outlined above for increasing the accuracy of the determined kinetic parameters. A first approach is to perform an additional experiment using a tighter range of substrate concentrations (e.g. using 1.7-fold dilutions from 5× the estimated K_M: 5×, 2.9×, 1.7×, 1.0×, 0.60×, 0.35×, 0.21X×K_M) and combining these data with the data collected in step 13 (Figure 9.23c).

9.4.2.4 Determining the Mechanism of the Bisubstrate Enzyme

19. Perform a series of rate experiments in triplicate using different concentrations of substrates *A* and *B*. Perform these at sets of eight concentrations of substrate *A*, using twofold dilutions from 8× the K_M determined in step 14 as above with a no substrate control. Perform five sets of experiments, using substrate *B* concentrations of 0.25×, 0.5×, 1×, 2×, 4× the K_M determined in step 16 (Figure 9.24). The outcome of this experiment is independent of whether substrate *A* or *B* has more concentrations tested, so it is perfectly valid to choose either substrate as *A* for the purpose of this assay.
20. Fit the data obtained to the models for ping-pong and sequential reaction mechanisms (Figure 9.25a). If the data fit better to the ping-pong model, this identifies the mechanism as a ping-pong mechanism. If the data fit better to the sequential model, proceed to step 21 to determine which type of sequential mechanism is preferred. In comparing the models, consider how strong the discrimination is. The selected model

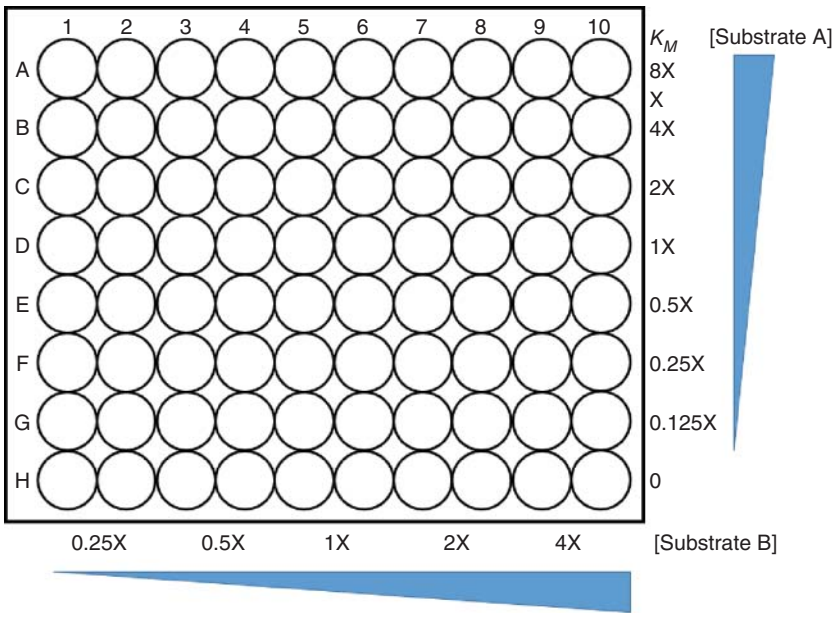

Figure 9.24 Design of the experiment to determine the bisubstrate enzyme mechanism. Suggested plate setup for the experiment, using values from earlier experiments to guide substrate concentrations. For continuous reactions, the plate will likely need to be split into several tests for convenience.

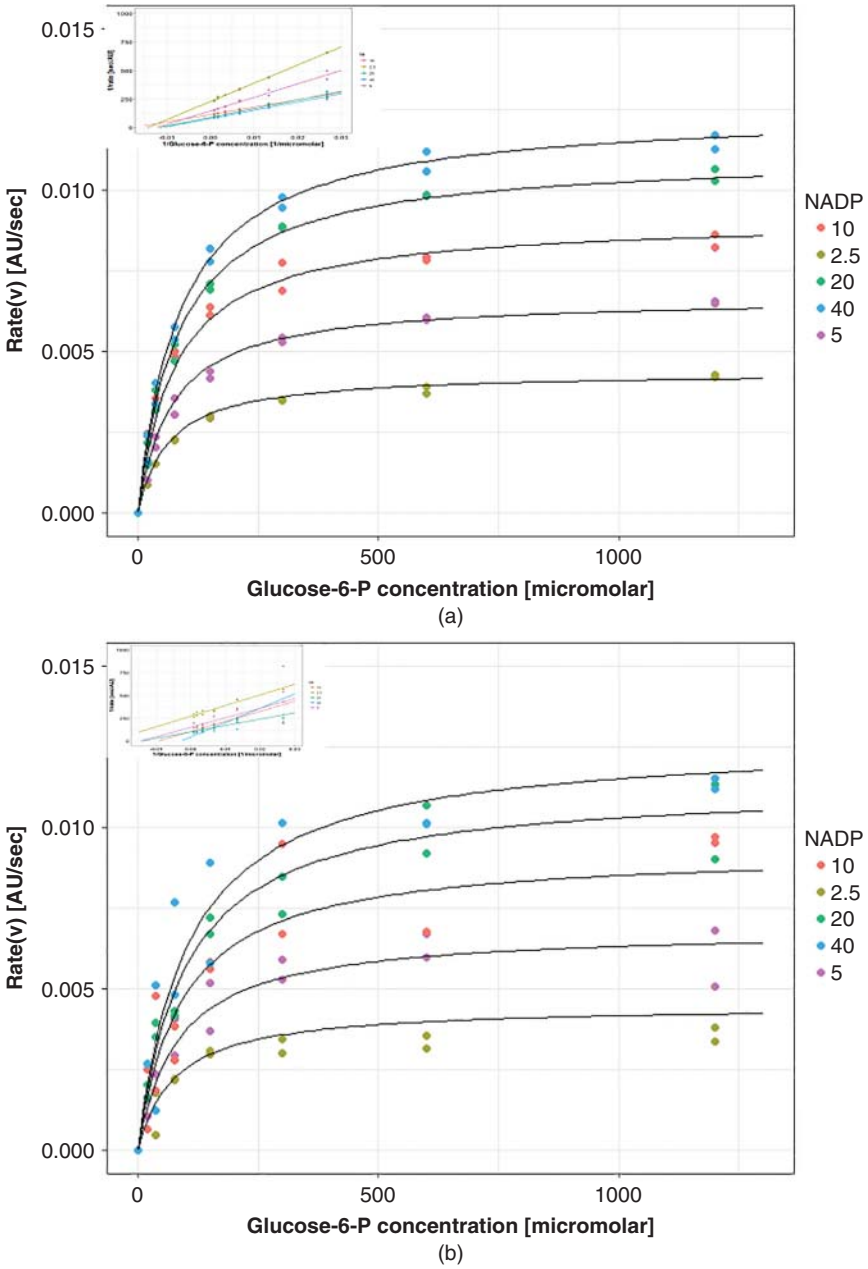

Figure 9.25 Experiments to determine bisubstrate enzyme mechanism. Examples with *L. mesenteroides* glucose-6-phosphate dehydrogenase, varying the concentration of glucose-6-phosphate and $NADP^+$. Here, twofold dilutions of glucose-6-phosphate are shown from a starting concentration of 1200 μM (C1–C7; 1200 μM represents 8× the estimated value of $K_{M\,app}$ from an initial experiment) and five twofold dilutions of $NADP^+$ from a starting concentration of 40 μM (40 μM represents 4× the estimated value of $K_{M\,app}$; this would be practically challenging to achieve as the $K_{M\,app}$ is low, and the reaction would proceed to completion rapidly). Models include random errors in substrate concentrations added and measurements to simulate experimental data. (a) Model data fit better to the sequential model than the ping-pong model (consistent with the method used to generate the model; Akaike's information criterion gives $p = 4 \times 10^{-9}$). Inset: Lineweaver–Burk plot of the same data. (b) Model data with increased errors. These data give an equivocal differentiation between the models (Akaike's information criterion: $p > 0.2$; implemented using RStudio). Inset: Lineweaver–Burk plot of the same data is not discriminating.

should show a significantly better fit than the alternative model. Where the discrimination is equivocal, it may be necessary to collect a wider range of data (Figure 9.25b).

9.4.2.5 Determining which Sequential Mechanism Is Adopted by a Bisubstrate Enzyme

21. Perform a series of rate experiments in duplicate using different concentrations of substrate *A* and one product. Perform these at sets of eight concentrations of substrate *A*, using twofold dilutions from 8× the $K_{M\,app}$ determined in step 14 as above with a no substrate control. Perform five sets of experiments, using substrate *B* concentration of the $K_{M\,app}$ determined in step 16 and the relevant product at 0.25×, 0.5×, 1×, 2×, 4× the $K_{M\,app}$ of the respective substrate determined in steps 14 and 16 (Figure 9.26).
22. Repeat step 21 with the second product, if it is possible to obtain this.
23. Repeat steps 21 and 22, using substrate *B* at eight different concentrations with constant substrate *A*.
24. Fit the data obtained for each product with each substrate to the competitive, uncompetitive and non-competitive models of inhibition (Figure 9.26b). Select the model that provides the best fit. In comparing the models, consider how strong the discrimination is. The selected model should show a significantly better fit than the alternative model. Where the discrimination is equivocal, it may be necessary to collect a wider range of data.
25. Compare the obtained results to Table 9.1. This should indicate whether the enzyme adopts a rapid equilibrium random sequential mechanism or an ordered sequential mechanism.

9.5 Case Study: Determination of Michaelis–Menten Parameters for a Bisubstrate Enzyme

Polysaccharides (PS) are macromolecules formed from chains of sugar monosaccharides linked through condensation of hydroxyls on pairs of sugars (Figure 9.27) [51]. These macromolecules have a wide range of important roles in cellular behaviour and homeostasis [52]. PS are essential for the biology of many bacteria, in particular helping to modulate the immune system [53, 54]. Consequently, PS are commonly used as vaccines for infectious disease [55–57] and the enzymes that synthesise them have been proposed as targets for next generation antimicrobials [58, 59]. Understanding mechanism and kinetic parameters for such enzymes is important for this drug design: compounds binding to the site of the first substrate in an ordered sequential mechanism will have greater effects than those binding to the second substrate, for example.

WcbL is a kinase from the tropical pathogen *Burkholderia pseudomallei* that catalyses the 1-phosphorylation of D-*manno*-heptose-7-phosphate (Figure 9.28) [60]. This forms part of the GDP-heptose biosynthesis pathway for formation of *B. pseudomallei*'s capsular polysaccharide [61–63]. Vivoli et al. solved the structure of the enzyme and characterised it biochemically [60]. Initial tests on the enzymes gave estimates for K_M as approximately 50 and 200 μM for D-*manno*-heptose-7-phosphate and ATP, respectively. However, a more detailed assay of the kinetics of ATP revealed a clear deviation from Michaelis–Menten kinetics (Figure 9.29a). Fitting these data to a cooperative model shows a Hill coefficient of 1.9 ± 0.1 (indicating near perfect cooperativity for the dimeric enzyme). This result required a second, more detailed assay to determine: consequently, the estimate of $K_{½}$ for the final experiment was well determined and close to the final, fitted result. The kinetics of the other substrate, D-*manno*-heptose-7-phosphate, also showed cooperativity (Figure 9.29b). In this case, the cooperativity is lower ($h = 1.5 \pm 0.1$). Furthermore, as this substrate shows, a low $K_{½}$ measuring the rates accurately at substrate concentrations lower than $K_{½}$ is challenging for the assay used. The deviation from Michaelis–Menten is far more subtle in this case and might well have been missed with a less accurate assay (as was indeed the case for the first enzyme in this pathway) [25, 62].

Crystal structures of WcbL identified the binding sites for the two substrates (Figure 9.30). The location of the binding sites suggested that the mechanism might be an ordered sequential reaction: the sugar–phosphate substrate binds deeply into the active site, while ATP binds over the active site and apparently blocks access to the sugar binding site. The enzyme was therefore tested using product inhibition. Here, one product

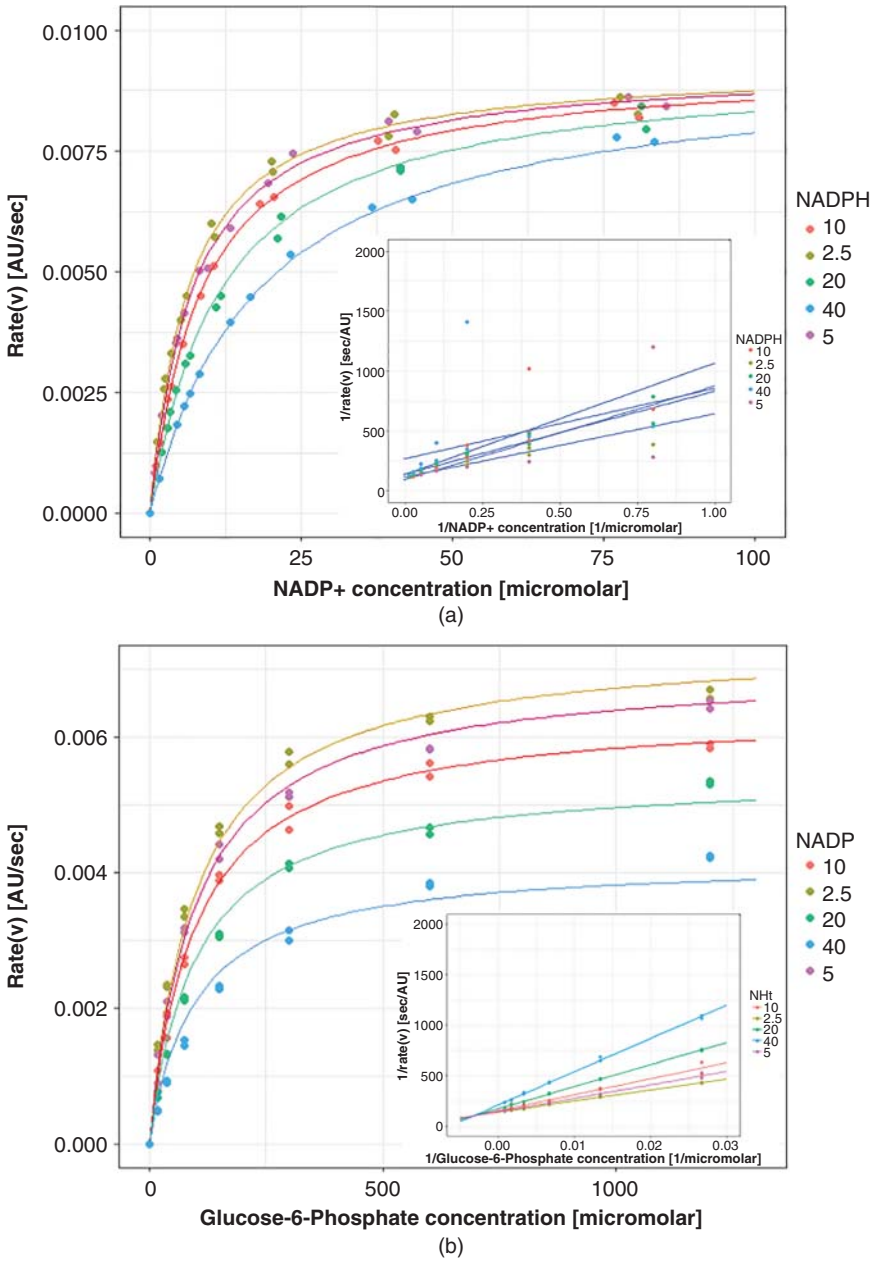

Figure 9.26 Experiments to determine the bisubstrate enzyme mechanism. Examples with *L. mesenteroides* glucose-6-phosphate dehydrogenase, using NADPH as a product inhibitor (the second product is insufficiently stable to use experimentally). Models include random errors in substrate concentrations added and measurements to simulate experimental data. (a) Experiments varying the concentration of $NADP^+$ at constant glucose-6-phosphate (150 μM). Twofold dilutions of $NADP^+$ are shown from a starting concentration of 80 μM and five twofold dilution of NADPH from a starting concentration of 40 μM. The model fits best to competitive inhibition (Akaike's Information Criterion; $p < 10^{-30}$). (b) Experiments varying the concentration of glucose-6-phosphate at constant $NADP^+$ (10 μM). Twofold dilutions of glucose-6-phosphate are shown from a starting concentration of 1200 μM and five twofold dilutions of NADPH from a starting concentration of 40 μM. The model fits best to non-competitve inhibition (Akaike's Information Criterion; $p < 10^{-11}$; implemented in RStudio). The corresponding Lineweaver–Burk plots are shown inset for reference.

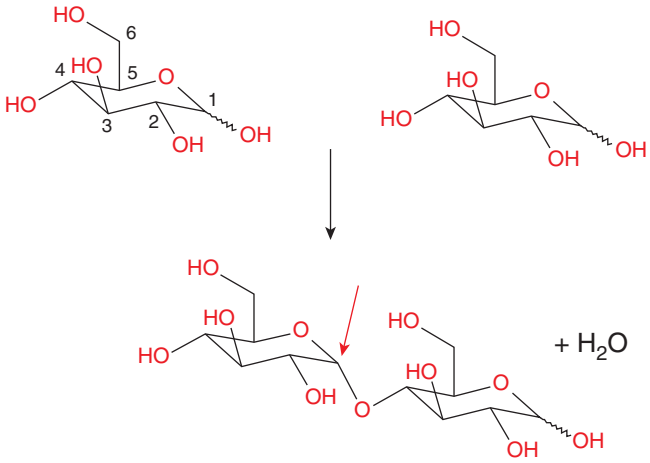

Figure 9.27 Basic structure of polysaccharides. Top left: a monosaccharide unit (glucose shown) has the generic formula $C_xH_{2x}O_x$. The most common have $x = 5–7$. Most sugars form rings as shown. The stereochemistry at positions 2–5 is fixed; position 1 has interchangeable stereochemistry in water. Two sugars can be polymerised by a condensation reaction, producing a disaccharide (bottom). Note that on polymerisation, the centre indicated by the red arrow now has fixed stereochemistry.

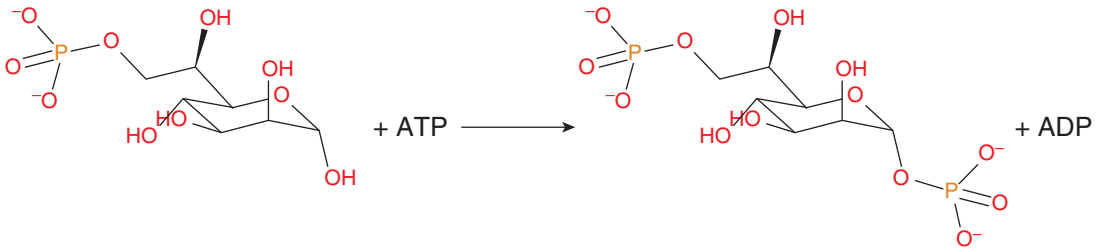

Figure 9.28 Overview of the WcbL reaction. The seven carbon sugars are used by bacteria in their surface polysaccharides.

(D-*manno*-heptose-1,7-bisphosphate) was not readily available. Consequently, only the other product (ADP) was tested. This showed non-competitive inhibition when varying the non-cognate sugar substrate and uncompetitive inhibition when varying ATP (at sugar concentrations well above K_M). In both cases, there was strong statistical support both for inhibition and for the selected mechanism over competitive inhibition. These data indicate an ordered, steady-state bisubstrate reaction (Table 9.1) and that ADP is expected to be the first product released (Figure 9.7a, blue square); no inhibition would be expected for an equilibrium ordered reaction and competitive inhibition for a rapid random equilibrium mechanism.

The experimental data on WcbL therefore provide strong evidence for the enzyme mechanism and for cooperativity in the enzyme. Similar mechanisms have been observed in other sugar kinases (e.g. [64, 65]). The kinetic and structural data here correlate very well, giving strong confidence in the conclusions of the kinetic studies.

9.6 More Advanced Methods

This chapter has described the determination of the steady-state kinetics of common enzymes. This is sufficient for many applications. Where additional insight is required, more advanced methods can

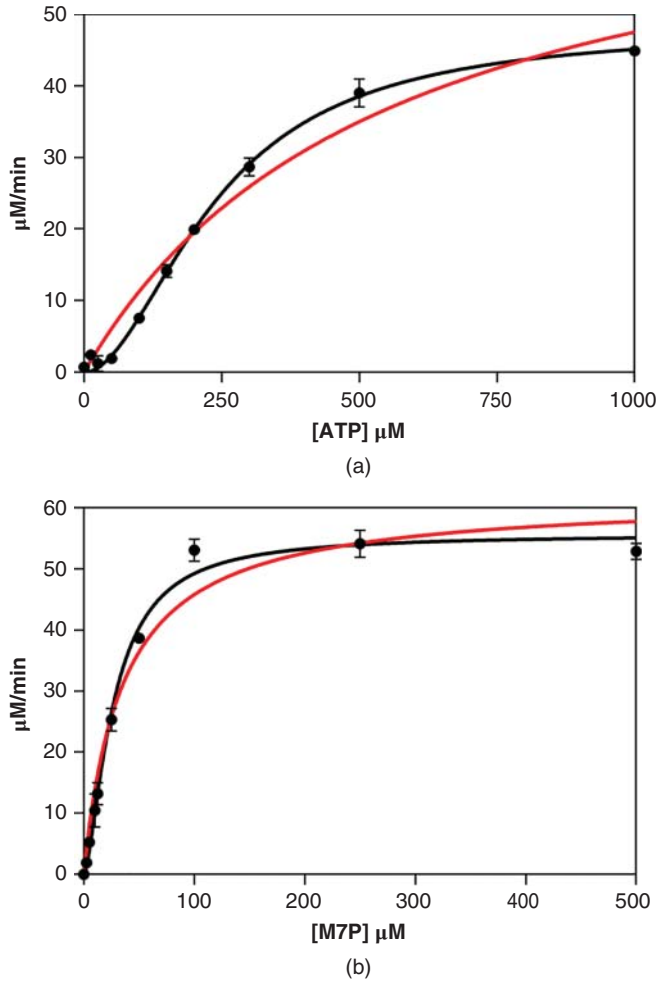

Figure 9.29 Enzyme activity of WcbL. (a) Activity of WcbL with ATP. Here, activity was tested at 10 ATP concentrations. The data show a clear deviation from Michaelis–Menten kinetics (red line). The Hill value h determined is 1.9 ± 0.1, indicating a high degree of cooperativity for a dimeric enzyme. (b) Activity of WcbL with the heptose substrate (M7P). This again shows cooperativity, although not to the same extent ($h = 1.5 \pm 0.1$).

be used. *Pre-steady state kinetics* uses instruments providing millisecond resolution (e.g. stopped-flow or quenched-flow). The time resolution and amount of data obtained allows determination of individual kinetic parameters rather than derivative parameters such as K_M [66, 67], allowing deep insight into mechanisms [68]. *Kinetic isotope effects* are observed when the isotope of one atom involved in the reaction is altered [19, 66]. The reaction rate generally slows when the mass of an atom involved in the reaction increases. Such reactions allow the experimenter to distinguish between possible reaction mechanisms, and potentially to identify rate-limited steps in reactions (e.g. [69]). Finally, structural methods (e.g. with free-electron lasers) are providing greater insight by following reactions with high time resolution after activating the enzyme (e.g. [70, 71]). These methods are currently only available for photoactivatable enzymes; further developments will increase the range of systems suitable for these studies.

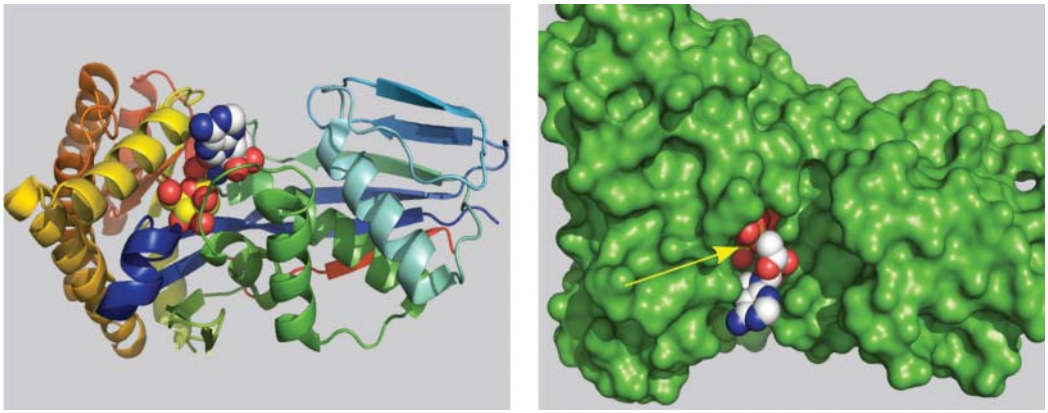

(a) (b)

Figure 9.30 WcbL binds to its substrates in an ordered manner. The structure of WcbL bound to substrate analogues reveals that the binding of ATP occludes the sugar binding site. (a) Cartoon representation of a WcbL monomer bound to both substrates. Mannose (phosphoheptose analogue) is shown as spheres with yellow carbons; AMP-PNP (ATP analogue) is shown as spheres with white carbons. (b) Surface representation of WcbL bound to substrates. ATP binds over the sugar binding pocket. One surface of the sugar can be observed in the occluded pocket (yellow arrow). The figure was prepared using PyMOL, based on PDB IDs 4UT4 and 4UTG [60].

9.7 Concluding Remarks

Biology requires the coordination of many enzyme reactions to operate efficiently. Today's medicine and biotechnology exploit our current understanding of enzymes to provide interventions and solutions. The increasing capabilities of microfluidics and robotics offer the potential to generate enzyme data at a significantly higher rate. This offers the opportunity to study enzymes in far greater detail, obtaining high quality data in smaller volumes at higher rates. These kinetic data can be used to optimise assays and in particular build enzyme cascades with ideal properties for a desired application. A thorough understanding of the properties of enzymes will underpin their use in diverse areas such as biotechnology (e.g. sensing), manufacturing (e.g. biocatalytic production of fine chemicals) and healthcare (e.g. diagnostic tests).

References

1 Erlandsen, H., Flatmark, T., Stevens, R.C., and Hough, E. (1998). Crystallographic analysis of the human phenylalanine hydroxylase catalytic domain with bound catechol inhibitors at 2.0 A resolution. *Biochemistry* 37 (45): 15638–15646.

2 Ranzani, A.T. and Cordeiro, A.T. (2017). Mutations in the tetramer interface of human glucose-6-phosphate dehydrogenase reveals kinetic differences between oligomeric states. *FEBS Lett.* 591 (9): 1278–1284.

3 Line, K., Isupov, M.N., and Littlechild, J.A. (2004). The crystal structure of a (−) gamma-lactamase from an Aureobacterium species reveals a tetrahedral intermediate in the active site. *J. Mol. Biol.* 338 (3): 519–532.

4 Blau, N., van Spronsen, F.J., and Levy, H.L. (2010). Phenylketonuria. *Lancet* 376 (9750): 1417–1427.

5 Mitchell, J.J., Trakadis, Y.J., and Scriver, C.R. (2011). Phenylalanine hydroxylase deficiency. *Genet. Med.* 13 (8): 697–707.

6 Cappellini, M.D. and Fiorelli, G. (2008). Glucose-6-phosphate dehydrogenase deficiency. *Lancet* 371 (9606): 64–74.

7 Kanehisa, M., Furumichi, M., Tanabe, M. et al. (2017). KEGG: new perspectives on genomes, pathways, diseases and drugs. *Nucleic Acids Res.* 45 (D1): D353–D361.
8 Blau, N., Belanger-Quintana, A., Demirkol, M. et al. (2009). Optimizing the use of sapropterin (BH(4)) in the management of phenylketonuria. *Mol. Genet. Metab.* 96 (4): 158–163.
9 Minucci, A., Moradkhani, K., Hwang, M.J. et al. (2012). Glucose-6-phosphate dehydrogenase (G6PD) mutations database: review of the 'old' and update of the new mutations. *Blood Cells Mol. Dis.* 48 (3): 154–165.
10 Luzzatto, L. and Seneca, E. (2014). G6PD deficiency: a classic example of pharmacogenetics with on-going clinical implications. *Br. J. Haematol.* 164 (4): 469–480.
11 Youngster, I., Arcavi, L., Schechmaster, R. et al. (2010). Medications and glucose-6-phosphate dehydrogenase deficiency: an evidence-based review. *Drug Saf.* 33 (9): 713–726.
12 Minucci, A., Giardina, B., Zuppi, C., and Capoluongo, E. (2009). Glucose-6-phosphate dehydrogenase laboratory assay: how, when, and why? *IUBMB Life* 61 (1): 27–34.
13 Bornscheuer, U.T., Huisman, G.W., Kazlauskas, R.J. et al. (2012). Engineering the third wave of biocatalysis. *Nature* 485 (7397): 185–194.
14 Reetz, M.T. (2013). Biocatalysis in organic chemistry and biotechnology: past, present, and future. *J. Am. Chem. Soc.* 135 (34): 12480–12496.
15 Bommarius, A.S. (2015). Biocatalysis: a status report. *Annu. Rev. Chem. Biomol. Eng.* 6: 319–345.
16 Wohlgemuth, R. (2010). Biocatalysis – key to sustainable industrial chemistry. *Curr. Opin. Biotechnol.* 21 (6): 713–724.
17 Wohlgemuth, R., Plazl, I., Znidarsic-Plazl, P. et al. (2015). Microscale technology and biocatalytic processes: opportunities and challenges for synthesis. *Trends Biotechnol.* 33 (5): 302–314.
18 Taylor, S.J.C., Mccague, R., Wisdom, R. et al. (1993). Development of the biocatalytic resolution of 2-Azabicyclo[2.2.1]Hept-5-En-3-one as an entry to single-enantiomer carbocyclic nucleosides. *Tetrahedron-Asymmetry* 4 (6): 1117–1128.
19 Cornish-Bowden, A. (2012). *Fundamentals of Enzyme Kinetics*. 4th, completely revised and greatly enlarged edition. ed., 498. Weinheim: Wiley-Blackwell.
20 Briggs, G.E. and Haldane, J.B. (1925). A note on the kinetics of enzyme action. *Biochem. J.* 19 (2): 338–339.
21 Cook, P.F. and Cleland, W.W. (2007). *Enzyme Kinetics and Mechanism*. London ; New York: Garland Science. 404 p.
22 Leskovac, V. (2003). *Comprehensive Enzyme Kinetics*. New York: Kluwer Academic/Plenum Pub. 438 p.
23 Koshland, D.E. Jr. and Hamadani, K. (2002). Proteomics and models for enzyme cooperativity. *J. Biol. Chem.* 277 (49): 46841–46844.
24 Koshland, D.E. Jr. (1996). The structural basis of negative cooperativity: receptors and enzymes. *Curr. Opin. Struct. Biol.* 6 (6): 757–761.
25 Vivoli, M., Pang, J., and Harmer, N.J. (2017). A half-site multimeric enzyme achieves its cooperativity without conformational changes. *Sci. Rep.* 7 (1): 16529.
26 Bloom, C.R., Kaarsholm, N.C., Ha, J., and Dunn, M.F. (1997). Half-site reactivity, negative cooperativity, and positive cooperativity: quantitative considerations of a plausible model. *Biochemistry* 36 (42): 12759–12765.
27 Cook, R.A. and Koshland, D.E. Jr. (1970). Positive and negative cooperativity in yeast glyceraldehyde 3-phosphate dehydrogenase. *Biochemistry* 9 (17): 3337–3342.
28 Ferrari, M.E., Fang, J., and Lohman, T.M. (1997). A mutation in *E. coli* SSB protein (W54S) alters intra-tetramer negative cooperativity and inter-tetramer positive cooperativity for single-stranded DNA binding. *Biophys. Chem.* 64 (1–3): 235–251.
29 Porter, C.M. and Miller, B.G. (2012). Cooperativity in monomeric enzymes with single ligand-binding sites. *Bioorg. Chem.* 43: 44–50.

30 Cornish-Bowden, A. (2014). Understanding allosteric and cooperative interactions in enzymes. *FEBS J.* 281 (2): 621–632.

31 Koshland, D.E. Jr. Nemethy, G., and Filmer, D. (1966). Comparison of experimental binding data and theoretical models in proteins containing subunits. *Biochemistry* 5 (1): 365–385.

32 Monod, J., Wyman, J., and Changeux, J.P. (1965). On the nature of allosteric transitions: a plausible model. *J. Mol. Biol.* 12: 88–118.

33 Cui, Q. and Karplus, M. (2008). Allostery and cooperativity revisited. *Protein Sci.* 17 (8): 1295–1307.

34 Domínguez de María, P., Stillger, T., Pohl, M. et al. (2006). Preparative enantioselective synthesis of benzoins and (R)-2-hydroxy-1-phenylpropanone using benzaldehyde lyase. *J. Mol. Catal. B Enzym.* 38: 43–47.

35 Muller, C.R., Perez-Sanchez, M., and Dominguez de Maria, P. (2013). Benzaldehyde lyase-catalyzed diastereoselective C–C bond formation by simultaneous carboligation and kinetic resolution. *Org. Biomol. Chem.* 11 (12): 2000–2004.

36 Apweiler, R., Armstrong, R., Bairoch, A. et al. (2010). A large-scale protein-function database. *Nat. Chem. Biol.* 6 (11): 785.

37 Lineweaver, H., Burk, D., and Deming, W.E. (1934). The dissociation constant of nitrogen-nitrogenase in Azotobacter. *J. Am. Chem. Soc.* 56: 225–230.

38 Harrison, R.K. and Stein, R.L. (1990). Substrate specificities of the peptidyl prolyl cis-trans isomerase activities of Cyclophilin and Fk-506 binding-protein – evidence for the existence of a family of distinct enzymes. *Biochemistry* 29 (16): 3813–3816.

39 Norville, I.H., Harmer, N.J., Harding, S.V. et al. (2011). A *Burkholderia pseudomallei* macrophage infectivity potentiator-like protein has Rapamycin-inhibitable peptidylprolyl isomerase activity and pleiotropic effects on virulence. *Infect. Immun.* 79 (11): 4299–4307.

40 Reed, M.C., Lieb, A., and Nijhout, H.F. (2010). The biological significance of substrate inhibition: a mechanism with diverse functions. *Bioessays* 32 (5): 422–429.

41 Copeland, R.A. (2000). *Enzymes : A Practical Introduction to Structure, Mechanism, and Data Analysis*, 2e. New York: Wiley. 397p.

42 Fierke, C.A., Johnson, K.A., and Benkovic, S.J. (1987). Construction and evaluation of the kinetic scheme associated with dihydrofolate reductase from *Escherichia coli*. *Biochemistry* 26 (13): 4085–4092.

43 Burnham, K.P. and Anderson, D.R. (2004). Multimodel inference – understanding AIC and BIC in model selection. *Sociol. Method Res.* 33 (2): 261–304.

44 Burnham, K.P., Anderson, D.R., and Burnham, K.P. (2002). *Model Selection and Multimodel Inference : A Practical Information-Theoretic Approach*, 2e. New York: Springer. 488p.

45 Naylor, C.E., Gover, S., Basak, A.K. et al. (2001). NADP(+) and NAD(+) binding to the dual coenzyme specific enzyme *Leuconostoc mesenteroides* glucose 6-phosphate dehydrogenase: different interdomain hinge angles are seen in different binary and ternary complexes. *Acta Crystallogr. D Biol. Crystallogr.* 57: 635–648.

46 Cosgrove, M.S., Cover, S., Naylor, C.E. et al. (2000). An examination of the role of Asp-177 in the His-Asp catalytic dyad of *Leuconostoc mesenteroides* glucose 6-phosphate dehydrogenase: X-ray structure and pH dependence of kinetic parameters of the D177N mutant enzyme. *Biochemistry* 39 (49): 15002–15011.

47 Levy, H.R. (1989). Glucose-6-phosphate dehydrogenase from *Leuconostoc mesenteroides*. *Biochem. Soc. Trans.* 17 (2): 313–315.

48 Olive, C., Geroch, M.E., and Levy, H.R. (1971). Glucose 6-phosphate dehydrogenase from *Leuconostoc mesenteroides*. Kinetic studies. *J. Biol. Chem.* 246 (7): 2047–2057.

49 Cosgrove, M.S., Naylor, C., Paludan, S. et al. (1998). On the mechanism of the reaction catalyzed by glucose 6-phosphate dehydrogenase. *Biochemistry* 37 (9): 2759–2767.

50 Levy, H.R., Christoff, M., Ingulli, J., and Ho, E.M.L. (1983). Glucose-6-phosphate-dehydrogenase from Leuconostoc-Mesenteroides – revised kinetic mechanism and kinetics of Atp inhibition. *Arch. Biochem. Biophys.* 222 (2): 473–488.

51 Varki, A. and Kornfeld, S. (2015). Historical background and overview. In: *Essentials of Glycobiology* (ed. A. Varki, R.D. Cummings, J.D. Esko, et al.), 1–18. NY: Cold Spring Harbor.

52 Varki, A. and Gagneux, P. (2015). Biological functions of Glycans. In: *Essentials of Glycobiology* (ed. A. Varki, R.D. Cummings, J.D. Esko, et al.), 77–88. NY: Cold Spring Harbor.

53 Mazmanian, S.K. and Kasper, D.L. (2006). The love-hate relationship between bacterial polysaccharides and the host immune system. *Nat. Rev. Immunol.* 6 (11): 849–858.

54 Neff, C.P., Rhodes, M.E., Arnolds, K.L. et al. (2016). Diverse intestinal bacteria contain putative zwitterionic capsular polysaccharides with anti-inflammatory properties. *Cell Host Microbe* 20 (4): 535–547.

55 Balmer, P., Borrow, R., and Miller, E. (2002). Impact of meningococcal C conjugate vaccine in the UK. *J. Med. Microbiol.* 51 (9): 717–722.

56 Jackson, L.A., Gurtman, A., van Cleeff, M. et al. (2013). Immunogenicity and safety of a 13-valent pneumococcal conjugate vaccine compared to a 23-valent pneumococcal polysaccharide vaccine in pneumococcal vaccine-naive adults. *Vaccine* 31 (35): 3577–3584.

57 Peltola, H. (2000). Worldwide *Haemophilus influenzae* type b disease at the beginning of the 21st century: global analysis of the disease burden 25 years after the use of the polysaccharide vaccine and a decade after the advent of conjugates. *Clin. Microbiol. Rev.* 13 (2): 302–317.

58 Taylor, P.L. and Wright, G.D. (2008). Novel approaches to discovery of antibacterial agents. *Anim. Health Res. Rev.* 9 (2): 237–246.

59 Tedaldi, L. and Wagner, G.K. (2014). Beyond substrate analogues: new inhibitor chemotypes for glycosyltransferases. *Medchemcomm* 5 (8): 1106–1125.

60 Vivoli, M., Isupov, M.N., Nicholas, R. et al. (2015). Unraveling the *B. pseudomallei* Heptokinase WcbL: from structure to drug discovery. *Chem. Biol.* 22 (12): 1622–1632.

61 Cuccui, J., Milne, T.S., Harmer, N. et al. (2012). Characterization of the *Burkholderia pseudomallei* K96243 capsular polysaccharide I coding region. *Infect. Immun.* 80 (3): 1209–1221.

62 Harmer, N.J. (2010). The structure of sedoheptulose-7-phosphate isomerase from *Burkholderia pseudomallei* reveals a zinc binding site at the heart of the active site. *J. Mol. Biol.* 400 (3): 379–392.

63 Reckseidler, S.L., DeShazer, D., Sokol, P.A., and Woods, D.E. (2001). Detection of bacterial virulence genes by subtractive hybridization: identification of capsular polysaccharide of *Burkholderia pseudomallei* as a major virulence determinant. *Infect. Immun.* 69 (1): 34–44.

64 Imriskova, I., Arreguin-Espinosa, R., Guzman, S. et al. (2005). Biochemical characterization of the glucose kinase from *Streptomyces coelicolor* compared to *Streptomyces peucetius* var. caesius. *Res. Microbiol.* 156 (3): 361–366.

65 Rivas-Pardo, J.A., Herrera-Morande, A., Castro-Fernandez, V. et al. (2013). Crystal structure, SAXS and kinetic mechanism of hyperthermophilic ADP-dependent glucokinase from *Thermococcus litoralis* reveal a conserved mechanism for catalysis. *PLoS One* 8 (6): e66687.

66 Fersht, A. (2017). *Structure and Mechanism in Protein Science : A Guide to Enzyme Catalysis and Protein Folding*. New Jersey: World Scientific. 631pp.

67 Johnson, K. (2003). *Kinetic Analysis of Macromolecules : A Practical Approach*. Oxford: Oxford University Press. 256pp.

68 Kellinger, M.W. and Johnson, K.A. (2010). Nucleotide-dependent conformational change governs specificity and analog discrimination by HIV reverse transcriptase. *Proc. Natl Acad. Sci. USA* 107 (17): 7734–7739.

69 Rankin, J.A., Mauban, R.C., Fellner, M. et al. (2018). Lactate Racemase nickel-pincer cofactor operates by a proton-coupled hydride transfer mechanism. *Biochemistry* 57 (23): 3244–3251.

70 Horrell, S., Kekilli, D., Sen, K. et al. (2018). Enzyme catalysis captured using multiple structures from one crystal at varying temperatures. *IUCrJ* 5 (Pt 3): 283–292.

71 Spence, J. and Lattman, E. (2016). Imaging enzyme kinetics at atomic resolution. *IUCrJ* 3: 228–229.